PhD Thesis in Materials and Structures Engineering

****

Comb-assisted high-sensitivity spectroscopy of molecular buffer gas cooled beams

****

in collaboration with the National Institute of Optics

INO-CNR of Naples

Valentina Di Sarno

Federico II, Naples

March 2016

dedication...

Al termine di questi tre anni di dottorato desidero ringraziare alcune delle persone che hanno fatto parte della mia vita, accompagnandomi in questo nuovo percorso di studio e ricerca e senza le quali non sarebbe stato possibile realizzare il presente lavoro di tesi.

Innanzitutto desidero ringraziare il mio amico e collega Luigi Santamaria Amato per avermi guidato nel percorso di ricerca con saggi consigli e preziosi suggerimenti. Gli sono immensamente grata per avermi seguito costantemente, sin dall'inizio, nello studio e in laboratorio e per il suo essere stato sempre diretto e sincero in ogni circostanza, condividendo le tante idee e i tantissimi dubbi e rendendomi partecipe di ogni progetto con il suo entusiasmo. Rappresenta per me un esempio di dedizione alla ricerca e un modello lavorativo certamente da perseguire.

Al mio Tutor Pasquale Maddaloni esprimo la mia riconoscenza per la fiducia che ha riposto in me, offrendomi la straordinaria chance di entrare a far parte di un Istituto scientifico stimolante come l'INO, trasmettendomi la sua esperienza professionale ed umana, facendomi sentire sempre parte del gruppo.

Vorrei inoltre esprimere tutta la mia gratitudine ai miei colleghi dell'INO, con i quali ho condiviso sempre momenti piacevoli, tanti pranzi e festeggiamenti, qualche gustoso seminario e diverse conferenze ma soprattutto ho sempre potuto contare sulla loro correttezza umana e collaborazione scientifica. Hanno sempre

condiviso incondizionatamente conoscenze e competenze preziose per lo svolgimento dell'esperimento.

Un ringraziamento speciale lo rivolgo senz'altro al mio tutor universitario e Coordinatore del dottorato di ricerca in Ingegneria dei Materiali, il Prof. Giuseppe Mensitieri che mi ha seguito in questi anni con i suoi importantissimi suggerimenti per il miglioramento del presente lavoro di dottorato.

Non posso, inoltre, non esprimere gratitudine verso i miei genitori i quali hanno sostenuto le scelte personali e professionali della mia vita e non hanno mai mancato di amore, ascolto e attenzione. Grazie infinite anche ai miei suoceri Aldo e Marina che mi hanno supportato in tanti modi nella vita privata e lavorativa e spronato ad andare avanti con grinta, facendomi sentire parte integrante della famiglia.

Infine, un ringraziamento speciale va a mio marito Roberto, per essermi stato sempre vicino, con il cuore e con la mente, cercando in ogni contesto della vita di confortarmi e rallegrarmi con il suo atteggiamento positivo e con la sua fiducia nella ricerca e nel prossimo.

Durante questo percorso di Dottorato mi sono cimentata in situazioni per me nuove con non pochi ostacoli da superare ma credo che il grado di soddisfazione personale sia proporzionale allo sforzo e all'impegno profuso lungo il cammino e non dipenda molto dal risultato raggiunto... Del resto, il dottorato non rappresenta nemmeno un punto di arrivo ma un nuovo inizio, l'inizio di una strada di ricerca (o almeno lo spero!) per cui, saluto questi miei tre anni di vita augurando a tanti altri ragazzi di avere la fortuna di intraprendere un percorso di studio ricco e stimolante, ma sopratutto supportato da colleghi di grande spessore scientifico e morale su cui poter contare.

Se qualcuno, leggendo questa tesi di dottorato, si chiedesse se vale la pena continuare studiare, provare a restare nell'ambito accademico o comunque quale possa essere un buon motivo per fare ricerca nonostante tutto, suggerisco la risposta che diede mio marito al Prof. Bozza, durante il suo esame di ammissione al Phd in Ingegneria Meccanica: "penso che lo studio elevi l'essere umano".

Abstract

In this thesis, continuous-wave cavity ring-down spectroscopy of a partially hydrodynamic molecular beam emerging from a buffer-gas-cooling source is demonstrated. Specifically, the $(\nu_1+\nu_3)$ vibrational overtone band of acetylene (C_2H_2) around 1.5 μm is accessed using a narrow-linewidth diode laser stabilized against a GPS-disciplined rubidium clock via an optical frequency comb synthesizer. As an example, the absolute frequency of the R(1) component is measured with a fractional accuracy of $\sim 4 \cdot 10^{-9}$. Our approach represents the very first step towards the extension of more sophisticated spectroscopic interrogation schemes, including Ramsey's method of separated fields, to buffer-gas-cooled molecular beams. It could also provide a powerful tool for spectroscopic characterization of molecular beams used in the epitaxial growth of thin films. Molecular Beam Epitaxy (MBE) is one of the most important growth facilities to grow epitaxial semiconductor materials for semiconductor optoelectronic devices, such as lasers, emitting diodes, detectors, and modulators.

Contents

List of Tables

List of Figures

Chapter 1

Sources of cold molecular beams

1.1 Introduction

During the past years, the possibility to investigate the low temperature behavior of stable molecules has motivated physicists, chemists and engineers from diverse backgrounds. Certainly, this development is inspired by the great successes in the closely related field of cold atoms which led to the demonstration of Bose-Einstein condensation in ultracold atomic gases in 1995.

Just like the production of ultracold ensembles of atoms has revolutionized the field of atomic and optical physics generating, in addition, much interest among researchers in other, traditionally disjoint fields, so the impact of creating cold (1 K - 1 mK) and ultracold (1 mK - 1 μK) molecules is expected to lead to discoveries reaching far beyond the focus of traditional molecular science [Carr et al. 2009].

Unfortunately, the cooling techniques so far developed for atomic species cannot be readily applied to molecules, because of the lack of a closed set of cycling transitions, due primarily to the absence of strict selection rules between vibrational levels.

At present, ultracold molecules can be obtained solely in the form of dimers, basically via magneto-association or photo-association of alkali atoms close to quantum degeneracy. However, a huge drawback of such indirect techniques is that

they only work with molecules whose constituent atoms can be laser cooled and trapped. Thus, for the conceivable future, many chemically relevant species (hydrides, nitrides, oxides, fluorides, etc.) will be still excluded. Meanwhile, a number of direct, more versatile approaches has been demonstrated to bring stable molecules into the cold temperature regime. Among these, the most successful methods are represented by buffer-gas cooling (BGC) and Stark deceleration (SD). In the former scheme, pioneered by J. Doyle's group, both translational and rotational degrees of freedom of the desired molecular species are cooled down to 4 K via elastic collisions with a thermal bath of helium (buffer gas) in a cryogenic cell [Maxwell 2005]. Then, a molecular beam is formed by allowing the molecules to escape into a high-vacuum environment via an orifice. The latter technique, invented by G. Meijer, relies on Stark-effect-based deceleration of a molecular beam via time-varying inhomogeneous electric fields arranged in a linear array [Vandemeerakker 2008]. Besides having already the potential to dramatically influence a variety of research domains encompassing precise control of chemical reactions, study of novel dynamics in low-energy collisions, and ultra-high-resolution molecular spectroscopy, output beams from either BGC or SD sources can serve as the underpinning for further trapping/cooling stages to approach the μK threshold.

Unexpected and largely unexplored physical phenomena occur in systems cooled to very low temperatures. The background temperature in the universe is approximately 2.7 K, but much lower temperatures have now been obtained in the laboratory, so collisions in this temperature regime attract great interest in the astrophysics and astrochemistry communities also. The lowest temperatures of interstellar space up to date are located around a Kelvin, which will reduce to even lower temperatures with the ongoing expansion of the universe. Here, cold molecular collisions in the laboratory can give insight into reactions of molecules in interstellar clouds for the present and future cosmic eras [Varanasi et al. 1983, Noll et al. 1986, Conrath et al. 1989].

1.2 Cold molecular beams

A molecular beam is a collimated stream of gas molecules with a well-defined spatial distribution, particle flux and energy distribution among the translational, vibrational, rotational and electronic degrees of freedom [Scoles 1988, Scoles 1992].

The first experiment with molecular beams, in 1911, confirmed a postulate of kinetic theory that molecules of a gas at a very low pressure travel in straight lines until they hit the walls of their container. At higher pressures, molecules have a shorter free path because they collide with each other before arriving at the wall. Because of the one-directional motion of the atoms or molecules, their properties can be studied in experiments that involve deflecting the beam in electric and magnetic fields or directing the beam onto a target. The target may be a solid, a gas, or a second beam of atoms or molecules. Ten years after, beams of polar molecules in an inhomogeneous electric field were investigated [Kallmann 1921] while in 1927 Erwin Wrede studied the relationship between dipole moments and deflection in a molecular beam [Zeitschrift 1927]. In 1939 Rabi invented a molecular beam magnetic resonance method to measure the magnetic moment of several lithium isotopes with molecular beams of LiCl, LiF and dilithium with two magnets placed one after the other to create an inhomogeneous magnetic field [Rabi et all 1939]. The use of beams to study chemical reactions and the transfer of energy between colliding molecules increased rapidly after 1955 [Herschbach 1976]. Also the invention of the maser by Gordon, Zeiger and Townes in 1957 was made with a molecular beam of ammonia and a special electrostatic quadrupole focuser [Gordon et all 1954]. Since the early days of spectroscopy, cold molecular beams, traditionally produced by supersonic jet expansion, have been employed. In this way the doppler broadening is suppressed and the particles are concentrated in the lowest vibration-rotation levels, improving significantly the quality of the absorption spectrum [Scoles 1988, Scoles 1992].

A new impetus to this research field is coming from the recent technologies for generating and manipulating beams of cold stable molecules, buffer-gas cooling (BGC) [Maxwell 2005, Patterson 2007, Sommer 2009, Hutzler 2012, Bulleid et al. 2013] and Stark deceleration [Bethlem 1999, vandeMeerakker 2008, vandeMeerakker 2012] above all. Besides having already the strength to dramatically influence the study of new dynamics in low-energy collisions and the accurate control of chemical reactions, these novel beam sources also serve as the starting point for further cooling and trapping stages. In this respect, opto-electrical cooling [Zeppenfeld 2012, Prehn 2016], laser chilling [Shuman 2010, Isaev 2016], and magneto-optical trapping [Hummon 2013, Norrgard 2016] represent the most promising candidates to approach the quantum degeneracy regime for the exploration of new Bose-Einstein condensation (BEC) features or quantum computing issues[Carr et al. 2009]. In parallel, thanks to the tremendous progress recently experienced in the field of high-resolution spectroscopy and absolute frequency metrology [Maddaloni book], equally disruptive searches, like that of the electric dipole-moment (EDM) of the electron [Hudson 2011, Baron 2013], the time variation of fundamental constants [Shelkovnikov 2008, Ubachs 2016] or the parity violation in chiral molecules [Tokunaga 2013], can be pursued exploiting the new potential of molecular beams [Carr et al. 2009]. Molecular beams are also one of most relevant tools for spectroscopy and studies of collisional processes [Morse 1996].

1.3 Theory of buffer gas cooling

As mentioned before there are many different methods to produce cold molecules because isn't possible a simple extension of the atomic laser-cooling technique due to the complex internal structure of molecules. The difficulty lies in finding sufficiently closed cycling transitions [H. J. Metcalf et all]. Since spontaneous emission of an electronically excited molecule is accompanied by a simultaneous vibrational transition that is not bound by strict selection rules, the vibrational state in the

excited electronic state is generally coupled to a large number of vibrational states in the electronic ground state. Buffer-gas cooling, before the laser-cooling technique, was used to cool down atomic hydrogen where the unique low binding energy of H to a liquid He surface has been exploited. Unfortunately, all other species have much higher binding energies with cold surfaces and, at the low temperatures required for loading a trap, all atoms would stick to the recipient walls. The solution to this problem is to use He as a buffer gas which is employed to thermalize the atoms by elastic collisions to temperatures below the trap depth before the particle touches the walls. When hot molecules are placed in a bath of cold atoms, their translational energy is quenched by elastic collisions with the buffer-gas atoms. After thermalization, the buffer-gas is pumped away, leaving a thermally isolated sample in the trap. As elastic collisions are independent of the internal structure, buffer-gas cooling provides a general method to cool atoms and molecules [J. M. Doyle et all].

1.3.1 Translational thermalization

Molecules are classified as cold or slow if their translational temperature is of the order or less than of a kelvin. In this section it's theoretically treat the cooling of the translational degrees of freedom of molecules by elastic collisions with buffer-gas atoms. Here, an inert buffer gas is enclosed in a container (buffer-gas cell), which is cooled to cryogenic temperatures by a refrigerator (helium refrigerator, pulse tube cooler etc.). Molecules enter the buffer-gas cell and dissipate their kinetic and internal energy through collisions with cold buffer-gas atoms. Cold beams of molecules can be created by making an exit aperture in one of the walls of the buffer-gas container(Figure 1.1).

The number of collisions that is needed to reduce the translational temperature of the molecules to the buffer-gas temperature for the translational degrees of freedom is derived in the following. The theoretical treatment is based on the model of hard-sphere elastic collisions. The model is schematically presented in Figure 1.2 .

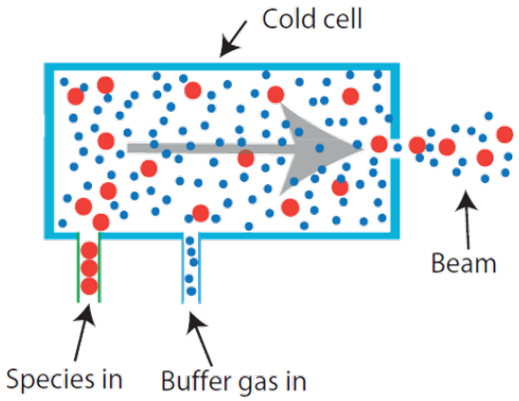

Figure 1.1: Buffer gas cooling cell

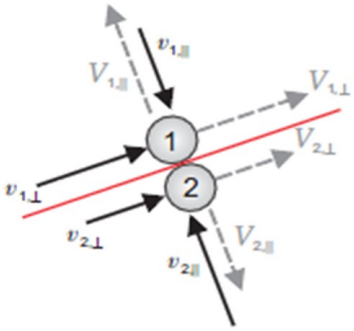

Figure 1.2: Velocity components in the hard-sphere elastic collision. The velocities before and after the impact are marked by black and grey arrows, respectively. Here, $\parallel$ and $\perp$ are the parallel and perpendicular velocity components to the line going through the centers of the two particles at the time of impact, respectively. The plane perpendicular to the line of centers is shown in red.

If we decompose the velocities of the two colliding partners in the lab frame prior (v_i) and after (V_i) the impact, respectively, into components which are parallel ($\parallel$) and perpendicular ($\perp$) to the line connecting the centers of the two particles at the time of impact, we have:

$$v_i = v_{i,\parallel} e_\parallel + v_{i,\perp} e_\perp, i \in 1, 2 \tag{1.1}$$

and

$$V_i = V_{i,\parallel} e_\parallel + V_{i,\perp} e_\perp, i \in 1, 2 \tag{1.2}$$

For hard sphere collisions, we obtain from momentum conservation:

$$m_1 v_1 + m_2 v_2 = m_1 V_1 + m_2 V_2 \tag{1.3}$$

Because the collision changes only the velocity components which are parallel to the line connecting the two centers at impact $\mathrm{v}_{i,\perp} = V_{i,\perp}$.

Thus the expression for momentum conservation in this case can be cast in the form:

$$m_1(v_{1,\parallel} - V_{1,\parallel}) = m_2(V_{2,\parallel} - v_{2,\parallel}) \tag{1.4}$$

On the other hand, from energy conservation

$$\frac{1}{2} m_1 V_1^2 + \frac{1}{2} m_2 v_2^2 = \frac{1}{2} m_1 V_1^2 + \frac{1}{2} m_2 V_2^2 \tag{1.5}$$

we obtain the relation:

$$v_{1,\parallel} + V_{1,\parallel} = V_{2,\parallel} + v_{2,\parallel} \tag{1.6}$$

Combining this relation with previous it is to express the velocities of the colliding partners after impact with the ones before impact:

$$V_{1,\parallel} = \frac{(m_1 - m_2) v_{1,\parallel} + 2 m_2 v_{_{2,\parallel}}}{m_1 + m_2} \tag{1.7}$$

$$V_{2,\parallel} = \frac{(m_2 - m_1) v_{2,\parallel} + 2 m_1 v_{_{1,\parallel}}}{m_1 + m_2} \tag{1.8}$$

Let us now apply the above model to the collision between a molecule and a buffer gas atom. Because the initial velocity of the buffer-gas atom v_2, is in general much smaller than the magnitude of the molecules velocity, we make the assumption that

$| v_2 | = 0$. This leads to

$$\Delta E = \frac{1}{2} m_2 V_2^2 = \frac{1}{2} m_1 (v_1^2 - V_1^2) \tag{1.9}$$

for the energy loss of the molecule per collision. If $E_{tot} = \frac{1}{2} m_1 v_1^2$ is the total collision energy, the fractional loss per collision is given by $\frac{\Delta E}{E_{Tot}} = \kappa^{-1}$

$$\kappa = \frac{v_1^2}{v_1^2 - V_1^2} = \frac{(m_1 + m_2)^2}{4 m_1 m_2} (\frac{v_1^2}{v_{1,\|}^2}) \tag{1.10}$$

where $(\frac{v_1^2}{v_{1,\|}^2})^{-1}$ is the angle of incidence θ between v_1 and the center line at the collision in the lab-frame. Because the $< cos^2\theta >= \frac{1}{2}$ we have

$$\kappa = \frac{(m_1 + m_2)^2}{2 m_1 m_2} \tag{1.11}$$

If each molecule experiences on average one collision with a buffer-gas atom the energy

$$E = \frac{3}{2} k_B \Delta T = \frac{3}{2} k_B (T_1 - T_2) \tag{1.12}$$

is removed from the thermal-molecular gas.

The temperatures of the molecular gas and the buffer gas before the two gases have collided are respectively T_1 and T_2. In contrast to the buffer gas, which is permanently cooled by the cell walls to the temperature T_2, the temperature of the molecules T will change in the mixture until $T = T_2$. The continuous change of temperature as a function of the average number of collisions N can be modeled by

$$\frac{dT}{dN} = -\frac{(T - T_2)}{\kappa} \tag{1.13}$$

Using the initial condition $T(0) = T_1$ the solution of the differential equation is given by

$$\frac{T(N)}{T_2} = (\frac{T_1}{T_2} - 1)e^{-N/\kappa} + 1 \tag{1.14}$$

The number of collisions needed for the temperature of the molecular gas to fall within a close vicinity of the buffer-gas temperature T_2 can be obtained from:

$$N = -\kappa ln \frac{T(N) - T_2}{T_1 - T_2} \tag{1.15}$$

It is desirable that the molecules have already thermalized to the buffer-gas temperature before they leave the cell through the exit aperture. Therefore, it must be guaranteed that the molecules have experienced a sufficient number N of collisions over the dimensions of the buffer-gas cell.

For example, for a helium buffer gas of $T \sim 8K$ and initially hot acetylene molecules of $T \sim 297K$, $N \sim 50$ collisions are needed to cool to the helium buffer-gas temperature.

1.3.2 Molecular beams emerging from a buffer-gas source

In contrast to elastic collisions, which govern translational relaxation, a simple expression for the number of collisions necessary for rotational thermalization cannot be found easily. The rotational relaxation rates depend strongly on the molecular structure. There are not many restrictions in the sense of collisional selection rules. Keeping this in mind we see that a transition from a highly excited rotational state to a lowly excited state is possible by a single collisional process if the cross section is sufficiently high. Therefore the steps needed to obtain thermalization are strongly dependent on the ratios of the cross-sections for the different relaxation channels and the thermal occupations at the beginning of the cooling process. The probability for a rotational deexitation step can be higher by many orders of magnitude compared to a vibrational relaxation step. After being cooled by collisions, most molecules will diffuse to the cell walls and stick. A small fraction will find the exit aperture and

form a beam. The beam parameters are determined by the dimensions of the buffer-gas cell, where the buffer-gas cooling takes place, the exit through which molecules leave the cell, as well as by the densities and temperatures of the buffer gas and the molecular gas in the cell.

In our experiments, the ratio between the densities of the molecules n_{mol} and the buffer-gas atoms n_{BG} is small. This guarantees that molecule molecule collisions can be neglected. The buffer-gas density n_{BG} is kept constant by continuously owing cold buffer gas into the buffer-gas cell. This is necessary because of the loss of atoms through the exit aperture.

1.4 Characterization of molecular flow regimes

The molecules in the gas are at first close enough together to interact with each other, but the gas expands in the vacuum until the molecules move independently.

Molecules in the beam move at various speeds; at low pressures of vapor in the box, when the free path of the molecules is greater than the width of the exit hole, the molecules will effuse through the hole while, at higher pressures, they will flow through the hole as fluids, forming a jet.

To characterize gas flow the Reynolds number is commonly used. It's defined as the ratio of inertial to viscous forces in a fluid flow:

$$R_e = \frac{F_{inertial}}{F_{viscous}} = \frac{\rho w^2 d^2}{\mu w d} = \frac{\rho w d}{\mu} \tag{1.16}$$

where ρ is the density, ω is the flow velocity, μ is the viscosity, and d is a characteristic length scale that in the case of beams is the aperture diameter. The possible types of flow can be roughly divided into three Reynolds number regimes (see Fig. 1.3) :

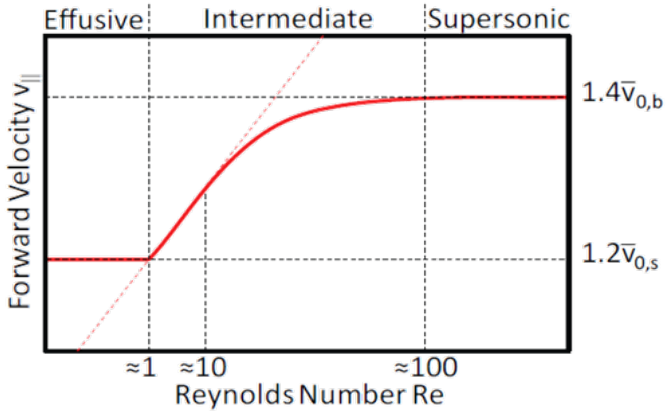

Figure 1.3: A schematic representation of beam forward velocity vs Reynolds number and buffer gas flow..

- Re $\leq$ 1: effusive regime. In this regime (low pressure), there are typically no collisions near the aperture, so the beam properties are simply a sampling of the thermal distribution present in the cell. The molecular velocities v are distributed according to the Maxwell Boltzmann equation:

$$f(v)dv = \frac{4}{\sqrt{\pi}}(\frac{m}{2k_BT})^{3/2}v^2e^{-\frac{mv^2}{2k_BT}} \tag{1.17}$$

When the molecules of an effusive beam are originated from a room-temperature container, the velocity is tipically a few hundred metres per second.

- $1 \leq Re \leq 100$: intermediate or partially hydrodynamic regime. Here there are enough collisions near the aperture to change the beam properties from those present in the cell but not enough so that the flow is fluid-like. Buffer gas beams typically operate in this regime; however, varing the geometrical and flow condition, buffer gas beams operate in all three regimes. Since the collisions near the aperture are primarily in the forward direction, the species can be accelerated, or boosted to a forward velocity, which is larger than the thermal velocity of the molecules (just as

with supersonic beams).

- $100 \leq Re$: fully hydrodynamic or supersonic regime. If the pressure in the container or the size of the hole is increased, the mean free path of the gas becomes smaller than the orifice. In this case, molecules escaping through the hole collide frequently, and adiabatic cooling of all degrees of freedom takes place in the expansion region. The total energy available per molecule in the gas in the container is converted into kinetic energy (directed flow), leading to supersonic beams of internally cold molecules [Christen 2010]. The buffer gas begins to behave more like a fluid, and the beam properties become similar to those of a beam cooled via supersonic expansion. The supersonic expansion technique can create cold beams of many species of atoms and molecules. The resulting beam is typically moving at a speed of several hundreds of m/s and usually, for a large class of species, has insufficient value of the flux for important applications.

A tipical schematic velocity distributions for selected effusive, supersonic, and buffer gas beam sources is showed in Fig. 1.4 [Hutzler et all 2012] :

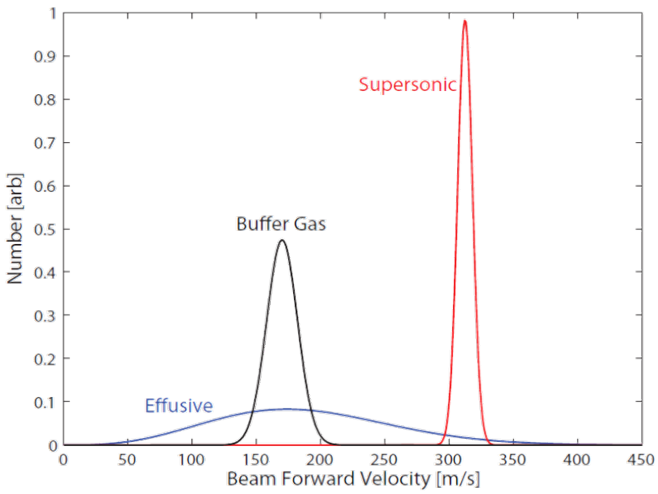

Figure 1.4: Schematic velocity distributions for selected effusive, supersonic, and buffer gas beam sources.

If molecules of nearly uniform speed are needed, the beam can be put through a filter called a velocity selector that permits only molecules within a small range of speeds to pass through. These selectors are often made of slotted disks or cylinders spinning rapidly on an axis parallel to the beam. The molecules that emerge from the selector are those with the right speed to stay in a given slot as they move along the cylinder. Molecules of other speeds are removed as they stick to or reflect from the sides of the slots. Changing the speed of rotation of the cylinder changes the speed at which the molecules are transmitted [Bart Wit].

1.5 Molecular Beam Deposition

When a a molecular beams is formed, molecules can arrive on a substrate from the material stream in a high vacuum. In this case, they can interact with the substrate in various ways, as it is illustrated in the schematic potential energy diagram in Figure 1.5. In the simplest case, the molecules can be:

- reflected back into the vacuum if they have too high energy which cannot be dissipated.
- chemisorbed if the molecule interacts more strongly with the surface (for example trough a covalent bond).
- physisorbed if there is only a weak Van der Waals interaction between the surface and the molecule.

When a molecule is adsorbed on a surface, it will sit at a position where the potential energy has a local minimum, the so called adsorption site. There are many different adsorption sites on any given surface and between different adsorption sites, there will be a potential energy barrier. The flux of molecules reaching the surface can generate a thin film.

The film growth technique rely on the molecular beam that transport materials from a source to the substrate through the vacuum (Figure 1.6). This material will

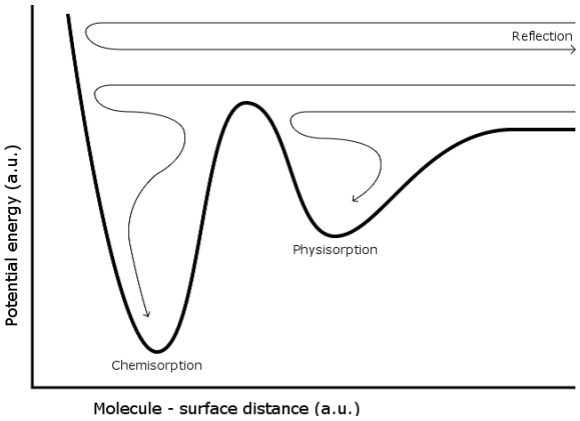

Figure 1.5: The potential energy curve in function of the distance of the molecule to the surface. Three important possible interactions are represented: physisorption, chemisorption and reflection.

be deposited on a given substrate and the value of the flux will contribute in the determination of the film growth rate. This technique is often referred to as MBE, where the E stands for Epitaxy.

MBE is an advanced ultra-high-vacuum facility to produce compound semiconductor materials with great purity (¿99.99999

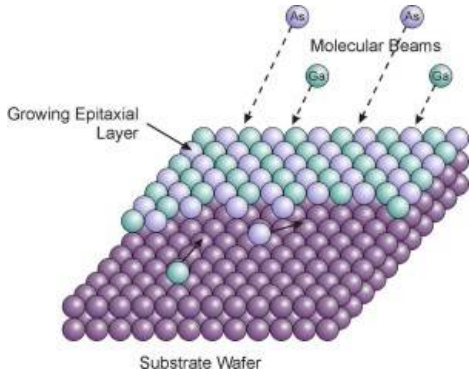

Figure 1.6: Epitaxial growth of monocrystalline layers.

In the conventional technique for the growth of thin layers of an organic material through deposition with molecular beam (OMBD), the material is simply evaporated or sublimed in the vacuum. The material can also be evaporated or sublimated inside a source containing a helium atmosphere; in this case, helium and molecules undergo a supersonic expansion into the vacuum (SuMBD). The principle difference

between OMBD and SuMBD lays in the way the molecular beam is generated and the properties of the beam itself.

1.5.1 Organic MBD

OMBD is based on thermal evaporation or sublimation of the target material in an ultra high vacuum. To this end, some highly pure material is placed into a Knudsen cell or a similar holder which can be heated. By heating the source material, it will either evaporate or sublime. In a Knudsen cell, an equilibrium will establish between the solid and the gas phase. A small amount of material is allowed to escape the cell into the vacuum such that this equilibrium is not affected. The escaped molecules will flow in a straight molecular beam. If the background pressure is maintained low, no collisions will occur and the molecules will continue in a straight line. By placing the substrate in the path of this flow, material will be deposited. The deposition rate is controlled by the source temperature. If the source temperature is higher, more molecules will go into the gas phase and more material will be deposited on the substrate. The temperature not only determines the deposition rate but also the energy distribution of the molecules.

Typically, the energy of the molecules is in the order of a few hundred meV. The distance from the source to the sample and the diameter of the orifice through which the molecules escape the Knudsen cell also influence the deposition rate, but these parameters are usually fixed. This distance and the orientation of the source with respect to the substrate are also quite important in determining the film uniformity. This is because the spatial distribution of the molecular flow is quite broad and not uniform. It is common practice to rotate the sample to make sure that the deposited film is as uniform as possible. Also, a shutter is used to control the deposition time and thus the film thickness. OMBD offers remarkable advantages [Tatti et all 2015] as a precisely controllable thermal evaporation, a seperate evaporation of each component and the substrate temperature is not high. Futhemore the growth rate is low ($1\mu m/h$)

so the profiles are ultrasharp, the surfaces are clean and free of an oxide layer. The drawbacks of this technique is that it's very expensive because is a very complicated system and the epitaxial growth is made under ultra-high vacuum conditions.

1.5.2 Supersonic MBD

Just like OMBD, the SuMBD technique uses a molecular beam to transport the desired material from the source to the substrate. However, this molecular beam is not a simple effusive flow as is the case with OMBD [Danman et all 2005] but it is a supersonic flow generated by a free jet expansion. This principle difference between the two techniques has significant implications for the properties of the beam and the deposited thin film. To generate a supersonic molecular beam, a specialized setup is required. First of all, one needs a custom built source. Typically, this is a tube made of quartz glass. Quartz is used because of the low thermal expansion coefficient, low thermal conductivity and because it is inert towards the commonly used materials. Inside this tube, an open capsule with the material is placed. A gas inlet is placed towards the back of the tube while at the front end of the tube, the nozzle is located. This source is placed inside an Ultra High Vacuum (UHV) chamber. Now, to generate a free jet expansion, gas is led into the source at relatively high pressure trough the gas inlet. At this point, there is a large pressure difference between the source and the high vacuum outside. Since there is an opening in the source, the gas will flow out and expand into the vacuum. This is the free jet expansion: it can be maintained if the amount of gas that flows into the UHV chamber is lower than the pumping capacity on that chamber [Xia et all 1995]. SuMBD offers some benefits over OMBD as a method for growing thin films. The most important one is the much higher kinetic energy of the molecules. When the molecules arrive at the surface, much of their kinetic energy is transferred to the internal degrees of freedom. However, part of the kinetic energy is conserved and the therefore the molecules will diffuse with hyperthermal velocities over the surface. Substrate phonons assure momentum conservation during

adsorption. Because of this, the molecules can diffuse much further over the surface before re-evaporating for the same surface temperature. Also, part of the energy is transferred to the substrate, or to an existing part of the film causing local annealing. This could also contribute to the higher quality of SuMBD grown films. Another, more subtle benefit is the possibility to change the kinetic energy of the molecules independently from the deposition rate. This is useful, because at higher deposition rates the film growth parameters can change as well. Also the beam collimation is advantageous because far less material is wasted this way. On the other side, a lot of carrier gas is used and the depositions are typically much slower for SuMBD growth [Podest et all 2000].

1.6 Molecular beam detection

In many case, the beam detection may be difficult because there are relatively few molecules in a typical beam and their velocities, and hence kinetic energies, are low. A detector should have high sensitivity, and there must be little interference from molecules coming from other sources, such as the residual gas in the vacuum chamber. Different kinds of detector are needed for different kinds of beam molecules. Useful solution during the 1950s combined electron impact ionization with mass spectrometry [Wessel and Lew 1953]. The great success achieved in molecular beam investigation on collision and surface science was favored by technical progress in ultrahigh vacuum tecnology and mass spectrometry. Atoms and molecules can be ionized by bombarding them with a stream of electrons, and the resulting ions can then be sorted and identified as to mass and charge by directing them into an instrument called a mass spectrometer [Pauly 2000]. Although versatile, a mass spectrometer is much less sensitive for alkali atoms than is the tungsten wire.

In the case of gas-phase spectra, most often the first barrier that is encountered is represented by collision broadening. Usually this is overcome simply by using samples at lower pressures. But soon after, the Doppler effect is the most severe

obstacle [Maddaloni 2013]. Laser spectroscopy has revolutionized this situation, currently allowing resolutions several orders of magnitude better than the Doppler limit. Indeed, many new high-resolution detection schemes have become feasible due to the high brightness, wide tunability, and narrow linewidth of lasers. High resolution is most often related to high-sensitivity detection. Just as an example, if the gas pressure is lowered to reduce pressure broadening, less signal is available, which can be compensated for by employing longer path lengths or diminishing the measurement noise. So, we shall also deal with some (the most effective ones) of those which are usually referred to as high-sensitivity spectroscopic techniques: a number of spectroscopic interrogation methods inherently possess the potential for both high-resolution and high sensitivity detection. Indeed, spectroscopic measurement precision increase dramatically with resolution, so the availability of a molecular-spectroscopy technique, able to combine the ultimate performance in terms of sensitivity, resolution, and frequency accuracy, can be crucial in many fundamental physical measurements.

In the last year a spectroscopic tecnique that has enabled high-sensitivity absorption detection of molecular beam was implemented in the INO laboratories. This very sensitive detection scheme is based on optical frequency comb-based cavity-ringdown spectroscopy (CRDS). In the field of precision spectroscopy and absolute frequency metrology, the effective and versatile CRDS technique reported here has an immediate, twofold impact on the field of molecular buffer gas cooling. In the wake of traditional supersonic beams, it enables a new generation of high-resolution ro-vibrational spectroscopic investigations on molecules of atmospheric or astrophysical interest and eventually, on the molecular beams for epitaxy experiments.

1.7 This thesis

In this PhD thesis the first implementation of a high sensitive CRD technique for ro-vibrational spectroscopy assisted by an optical frequency comb synthesizers on a molecular buffer gas cooled beams is described.

In particular, in chapter 2 the characterization of the cold acetylene gas ($^{12}C_2H_2$) inside a buffer gas cell at low-temperature is reported. It's described the BGC apparatus with ^{4}He (boiling point of $\simeq 4.2$ K at 1 atm) realized to prepare a $^{12}C_2H_2$ (boiling point of $\simeq 190$ K at 1 atm) sample at temperatures which are characteristic of the interstellar medium, concerning so, some astrophysical aspect. In this regime, laser absorption spectroscopy is performed, primarily aimed at determining, in conjunction with the outcomes of a Monte Carlo simulation, the total (as opposed to differential) elastic cross sections for the ^{4}He$-^{12}C_2H_2$ system.

In chapter 3 the measurement on a cold molecular beam of acetylene performed with the cavity ring down spectroscopy (CRDS) are described. CRDS measurements provides a very sensitive and accurate quantitative measurements of absorption features in the near-IR spectral region. To obtain an emission with absolutely frequency, the laser is locked to a self-referenced optical frequency comb synthesizer.

In chapter 4 a research proposals based on cold molecules technologies is exposed. It regards the monitoring of the eventual time variation of fundamental constants, measuring the time dependence of the ratio of the molecule frequency to any other standard frequency and extract the time dependence of the fundamental constants using the relation for the relative variations of dimensionless ratios. The generation of a beam of cold molecules will be the heart of the experiment.

Finally, the conclusion of the PhD activities are reported.

Chapter 2

Low-temperature spectroscopy of the $^{12}C_2H_2$ $(\upsilon_1 + \upsilon_3)$ band in a helium buffer gas cell

2.1 Introduction

By virtue of its prototypical role in different research areas, acetylene has been the subject of extensive spectroscopic studies [Herman et al. 2003, Herman et al. 2007]. First, the paradigmatic carbon-carbon triple bond provides a fertile ground for the exploration of fundamental quantum chemistry processes in molecular beams, including reactions and collisions as well as the formation of van der Waals complexes [Thibault et al. 2007, Thorpe et al. 2009, Didriche et al. 2012]. From a technological perspective, much work in the field of high-resolution spectroscopy has been motivated by the demand for improved frequency standards and metrological capabilities in the telecom spectral region [Edwards et al. 2005, Hardwick et al. 2006, Ryu et al. 2008, Ahtee et al. 2009]. Moreover, trace-molecule spectroscopy of acetylene is of considerable interest in atmospheric chemistry and geophysical research in connection with pollution control and global climate, respectively [Rinsland et al. 1987]. While

representing only a trace component on Earth, acetylene is formed, by photolysis of methane, in the atmospheres of giant planets (Jupiter, Saturn, Uranus, and Neptune) and Titan, as well as in various other stellar and interstellar environments [Varanasi et al. 1983, Noll et al. 1986, Conrath et al. 1989]; as such, acetylene is also a key species in astrophysics and astrobiology [Oremland & Voytek 2008].

Potentially profitable in all the above applications, laboratory spectroscopy investigations of acetylene in the low-temperature regime are crucial to understand and model planetary atmospheres. Indeed, it was thanks to the $^{12}C_2H_2$ ro-vibrational emission spectra at 13.7 μm (υ_5-fundamental band) observed by the instruments on board *Voyagers 1* and *2* that the atmospheric temperature of Jupiter (about 130 K), Titan (between 120 and 130 K), Saturn (around 90 K) and Neptune (below 60 K) were retrieved [Varanasi 1992].

More recently, infrared spectroscopic measurements performed by the Spitzer Space Telescope discovered trace amounts of acetylene in the troposphere of Uranus as well, consistent with a lowest recorded temperature of 49 K [Burgdorf et al. 2006]. While spectral lines in planetary atmospheres are mainly influenced by collisions with molecular hydrogen, atomic helium plays an important role, too. In this regard, calculations and measurements of collisional broadening and shift coefficients were specifically carried out for the helium-acetylene system, first on the mid-infrared ($\upsilon_4+\upsilon_5$) [Podolske & Loewenstein 1984] and υ_5 [Bouanich et al. 1991, Varanasi 1992, Babay et al. 1998, Heijmen et al. 1999] bands, respectively at 7.4 and 13.7 μm, and then on the near-infrared ($\upsilon_1 + 3\upsilon_3$) [Valipour & Zimmermann 2001] and ($\upsilon_1 + \upsilon_3$) [Thibault 2005, Arteaga et al. 2007, Bond et al. 2008] bands, at 788 nm and 1.5 μm, respectively; however, most of these studies focused on room-temperature systems, except for a couple of works reporting temperatures just below 195 [Bond et al. 2008] and 150 [Podolske & Loewenstein 1984] K. The general difficulty encountered in accessing the range of tens of Kelvin with laboratory spectroscopic setups lies in the fact that most of the species of interest, including acetylene, have poor vapor pressure in that temperature interval. Only in very few cases, based on

a special collisional cooling methodology, was such a limitation overcome and significantly lower temperatures, down to 4 K, reached [Messer & De Lucia 1984]. This allowed comprehensive investigations of pressure broadening in the CO-He system [Messer & De Lucia 1984], He-induced rotational relaxation of H_2CO [Ball & De Lucia 1998], and rotational inelastic cross sections for H_2S-He collisions [Mengel et al. 2000]. Nevertheless, this approach has never been applied to acetylene.

A new impetus to this research line comes from the emerging, powerful technologies for the cooling of stable molecules [Carr et al. 2009]. Among the various schemes, at least for temperatures in the few-Kelvin range, the buffer-gas-cooling (BGC) method is perhaps the most efficient in terms of produced sample density and it is applicable to nearly all molecules [Maxwell et al. 2005, Bulleid et al. 2013]. Here, a noble gas, typically helium, is chilled just above its boiling point and acts as a thermal bath (buffer) that cools in turn, through collisions, the injected molecular gas under analysis.

A thorough characterization of the BGC process is first accomplished, comprising measurements of translational temperatures by means of Doppler thermometry, as well as of internal (rotational) temperatures through the analysis of the relative intensities of several rotational lines.

These measurements reveal a situation that is very close to what is often found in the interstellar medium (ISM) which, while continuously ionized or excited by cosmic rays, is not sufficiently dense to guarantee complete thermalization of its constituent particles through collisions [Bradford et al. 2003]. Such a circumstance can be effectively realized in our BGC setup where, by properly changing the relevant experimental parameters (helium flux and cell size), the regime of borderline equilibrium between translational and rotational degrees of freedom can be continuously tuned towards more pronounced unbalances.

2.2 Experimental setup

The heart of the experimental apparatus is represented by a two-stage pulse tube (PT) cryocooler (Cryomech, PT415) housed in a stainless-steel vacuum chamber and fed with liquid helium by a compressor. The first (second) PT stage yields a temperature of 45 K (4.2 K) provided that its heat load is kept below 40 W (1.5 W); to guarantee this, each plate is enclosed in a round gold-plated copper shield, which suppresses black-body radiation effects. Capillary filling, regulated upstream by two flow controllers with an accuracy of 0.05 Standard Cubic Centimeters per Minute (SCCM), is used to inject both acetylene and helium, contained in room-temperature bottles, into the buffer cell. This latter consists of a gold-plated copper cube of side length $L_c = 54$ mm; it is in thermal contact with the 4.2-K plate and its exit hole has a radius of $r_h = 1$ mm. The acetylene pipe is made of stainless-steel and thermally insulated from both the PT stages; in addition, to avoid condensation, its temperature is maintained above 190 K by means of a proportional-integral-derivative (PID) feedback loop equipped with a silicon-diode thermometer as input sensor and an electric heater as output transducer. The buffer gas line comprises four connected segments: the first one is made of stainless-steel and consists of several windings in order to keep the heat conductance as low as possible; then, a bobbin-shaped copper tube is secured to the 45-K plate; the third segment, identical to the first duct, minimizes thermal exchanges between the two PT stages; finally, a second spool-shaped copper pipe is fixed to the 4.2-K plate, intended to cool the helium gas down to a few K before entering the buffer cell. A second PID controller is also implemented for fine tuning of the buffer cell temperature. To keep the pressure within the radiation shields below 10^{-7} mbar, the internal surface of the inner shield is covered with a layer of activated charcoal that, at cryogenic temperatures, acts as a pump (with a speed of a few thousands dm^3/s) for helium and non-guided molecules; the gas adsorbed by the charcoal is released during warm up of the cryogenic system and then pumped out of the vessel by a turbomolecular pump. As shown in Fig. 3.3,

both the vacuum chamber, the shields and the buffer cell have optical accesses for spectroscopic interrogation.

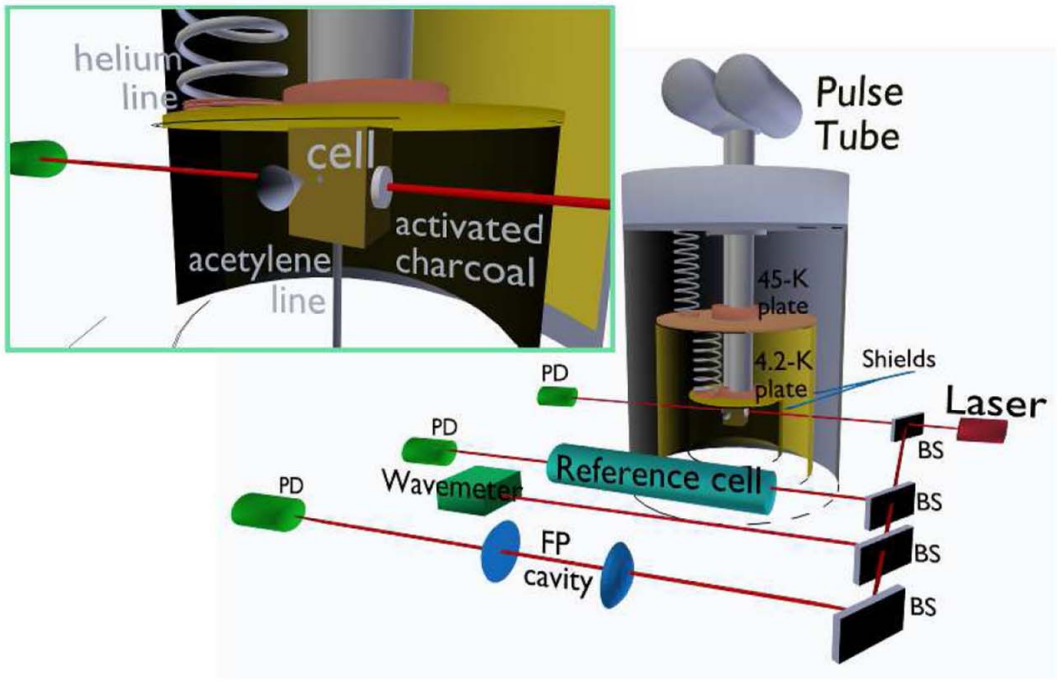

Figure 2.1: Layout of the experimental setup including a zoom on the buffer-gas cell. Laser absorption spectroscopy is used to characterize collisional cooling of $^{12}C_2H_2$ in a ^{4}He thermal bath down to a temperature of few Kelvin.

The probe radiation source is an external-cavity (Littman-Metcalf configuration) diode laser emitting several milliwatts of power between 1520 and 1570 nm with a linewidth below 1 MHz (New Focus, TLB-6300 Velocity). The laser output beam is split into four parts: one portion is sent to a room-temperature cell containing acetylene in order to identify the various transitions; a second beam is coupled to a confocal, Fabry-Perot (FP) interferometer for frequency calibration purposes; a third fraction is delivered to a wavelength meter with an accuracy of 0.2 ppm (Burleigh WA-1500); the last part passes through the buffer gas cell and is eventually collected by an InGaAs photo-detector (PD). The molecular absorption profile, $\delta(\nu) \equiv [I_0 - I(\nu)]/I_0$,

is recovered by scanning the laser frequency ν through the application of a linear-ramp voltage to the piezoelectric transducer attached to the external-cavity tuning element.

2.3 Measurements and analysis

2.3.1 Translational temperatures

In order to monitor the collisional cooling process, the absorption spectrum of the R(5) ro-vibrational transition in the $(\upsilon_1 + \upsilon_3)$ band (henceforth referred to as transition a) was acquired under different experimental conditions, by varying the buffer-cell temperature, T_{cell}, and the two gas flows, f_{He} and $f_{\mathrm{C_2H_2}}$. Since the translational temperature, T_{trans}, in a gas is related to the mean square velocity of its molecules, each observed absorption profile was fitted by a Gaussian distribution

$$G(\nu) = G_0 \exp\left[-\frac{4\,\ln 2\,(\nu-\nu_0)^2}{\sigma_D^2}\right] \tag{2.1}$$

where the amplitude G_0, the transition center frequency ν_0, and the Doppler width $\sigma_D = (\nu_0/c)\sqrt{8\ln 2\, m^{-1} k_B T_{trans}}$ represent the fitting parameters (here, m is the molecular mass, c the light speed, and k_B the Boltzmann constant). Thus, the translational temperature of the acetylene sample was retrieved by the extracted σ_D value. The same procedure was repeated for several ro-vibrational lines, including the R(1) component, leading to the same Gaussian widths (within the errors) under equal conditions. As an example, three absorption spectra are shown in Fig. 2.2, corresponding to the following T_{cell} values: 294, 115 and 10 K; for $T_{cell} = 294$ K, only 1 SCCM of acetylene was let into the cell and no helium; for $T_{cell} = 115$ K, $f_{\mathrm{He}} = 20$ SCCM and $f_{\mathrm{C_2H_2}} = 5$ SCCM were used; for $T_{cell} = 10$ K, $f_{\mathrm{He}} = f_{\mathrm{C_2H_2}} = 2$ SCCM was found to be the optimal choice to reach the translationally coldest sample with our setup: $T_{trans} = 15 \pm 3$ K.

Concerning the 15-K curve, the fit residuals look like a white-noise floor, a slight deviation from this behavior being found only in the tails which, however, contribute very marginally to the extraction of the fit parameters. Supported by a temperature reading of 15 K recorded on the He pipe just before the entrance into the buffer cell, the discrepancy at the lowest temperature was attributed to a non-perfect thermal exchange between the copper pipe and the two PT plates; to bridge this gap, an improved setup for better cooling of the He line is already under construction. It should be noted that equal flows of the two gases do not correspond to equal densities in the buffer cell. In fact, many of the acetylene molecules freeze upon impact on the walls (as well as on the optical windows), hence generating a layer of solid acetylene whose thickness increases with time. This is not the case for the helium. Nonetheless, after a short transient (less than 10 ms in the worst case), stationary gas densities, n_{He} and $n_{\mathrm{C_2H_2}}$, namely gas pressures, will be established inside the buffer cell, leading to steady-state spectroscopic absorption profiles; these will eventually disappear as soon as the optical windows fog up. It is also worth remarking here that, in the work presented here, the stationary cell gas pressures were always lower than 0.2 mbar, giving rise to negligible pressure broadening and shift effects. In fact, the helium-induced pressure broadening coefficients of the acetylene R(1) and R(5) lines are respectively 3.1598 and 2.9970 MHz/mbar [Bond et al. 2008], corresponding to a maximum broadening of about 600 kHz, well below the resolution of our spectrometer (a few MHz).

2.3.2 Rotational temperatures

The linestrength of a given ro-vibrational transition depends on the rotational temperature, T_{rot}, hereafter simply called T to simplify the notation, through the

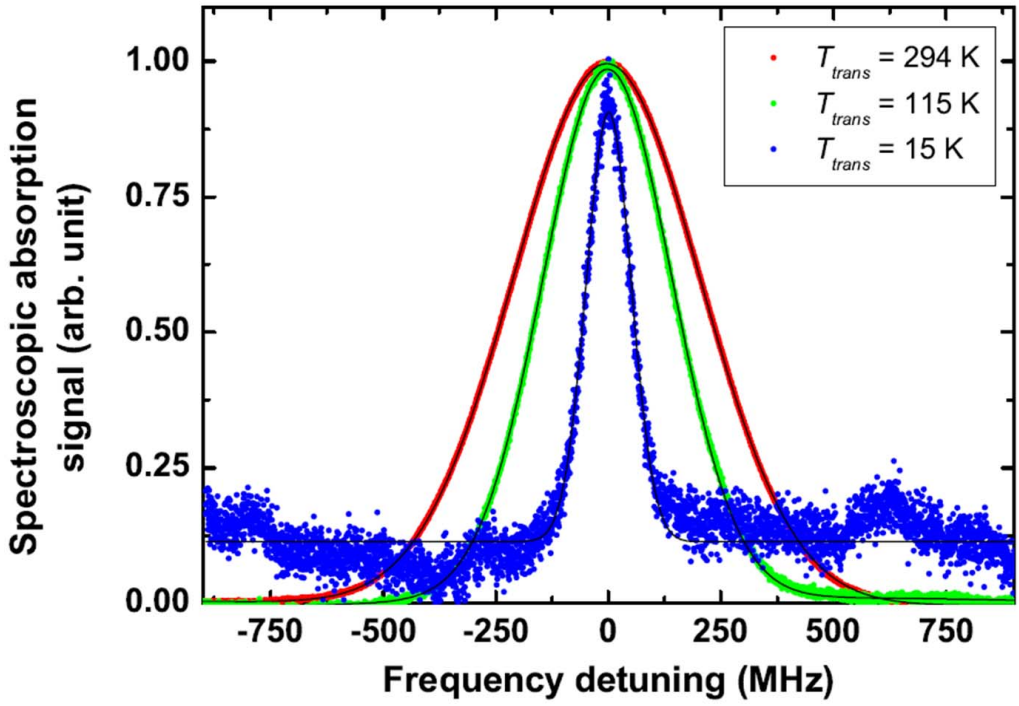

Figure 2.2: Spectroscopic absorption signals (normalized to unit) obtained for transition a in correspondence with the following triplets: $T_{cell} = 294$, $f_{\mathrm{He}} = 0$ SCCM, $f_{\mathrm{C_2H_2}} = 1$ SCCM; $T_{cell} = 115$, $f_{\mathrm{He}} = 20$ SCCM, $f_{\mathrm{C_2H_2}} = 5$ SCCM; $T_{cell} = 10$, $f_{\mathrm{He}} = 2$ SCCM, $f_{\mathrm{C_2H_2}} = 2$ SCCM. The extracted translational temperatures are: 294 ± 2, 115 ± 5, 15 ± 3 K, respectively.

relationship [Rothman et al. 1998]

$$S(T) = S(T_{ref})\frac{Q(T_{ref})}{Q(T)}\frac{\exp\left(\frac{-c_2 E_f}{T}\right)}{\exp\left(\frac{-c_2 E_f}{T_{ref}}\right)}\frac{1-\exp\left(\frac{-c_2\nu_0}{T}\right)}{1-\exp\left(\frac{-c_2\nu_0}{T_{ref}}\right)}\ , \tag{2.2}$$

where T_{ref} is a reference rotational temperature at which the linestrength is known, $Q(T)$ the rotational partition function (varying between 3 at 10 K and 100 at 294 K in the case of acetylene [Amyay et al. 2011]), E_f the transition's lower-level energy (expressed in wavenumbers), and $c_2 = hc/k_B$ (h is the Plank constant). Eq. 2.2 was exploited to perform accurate measurements of rotational temperatures according to

the following procedure. First, besides transition a (at $\nu_{0a} = 6570.042687$ cm^{-1}), the $(\upsilon_1 + \upsilon_3)$ R(1) component, called transition b (at $\nu_{0b} = 6561.094106$ cm^{-1}), was also selected so that the ratio between the two respective linestrengths,

$$R_{ba}(T) \equiv \frac{S_b(T)}{S_a(T)} = \frac{\frac{\exp\left(\frac{-c_2 E_{fb}}{T}\right)}{\exp\left(\frac{-c_2 E_{fb}}{T_{ref}}\right)} \frac{1-\exp\left(\frac{-c_2 \nu_{0b}}{T}\right)}{1-\exp\left(\frac{-c_2 \nu_{0b}}{T_{ref}}\right)}}{\frac{\exp\left(\frac{-c_2 E_{fa}}{T}\right)}{\exp\left(\frac{-c_2 E_{fa}}{T_{ref}}\right)} \frac{1-\exp\left(\frac{-c_2 \nu_{0a}}{T}\right)}{1-\exp\left(\frac{-c_2 \nu_{0a}}{T_{ref}}\right)}} \quad , \tag{2.3}$$

exhibits a steep slope below a few tens of Kelvin (see Fig. 2.3), whereas it displays a lowly slope for higher temperatures. This reduces errors in the determination of low rotational temperatures. In a sense, by giving up resolution in the high-temperature region, a fair resolution in the low-temperature interval is obtained, even better than that achieved for translational temperatures.

Second, for different T_{trans} values, the experimental value of $R_{ba}(T) \equiv S_b(T)/S_a(T) = \int \delta_b(\nu)\, d\nu / \int \delta_a(\nu)\, d\nu$ was determined. This value, along with the E_f's and ν_0's parameters provided by the Hitran database [Hitran], was replaced in Eq. 2.3 which was finally solved for T.

In conclusion, the minimum observed rotational temperature was $T = (20 \pm 1)$ K for a measured translational temperature of $T_{trans} = (15 \pm 3)$ K; such a difference is compatible with the fact that cooling is more efficient for the translational degrees of freedom than for rotational ones [Maddaloni book], albeit the two measured temperature values are consistent within 2 standard deviations. As anticipated, such a temperature gap can be deliberately enhanced by reducing the cell size or increasing the helium flux, thus enabling the exploration of different intermediate regimes up to a non equilibrium.

In general, unlike what happens to translational states, even if the initial distribution over the rotational states is Boltzmannian, it will relax without preserving the canonical invariance, and it will not be possible to define a rotational temperature [Sanna]. The necessary conditions so that the canonical invariance is maintained

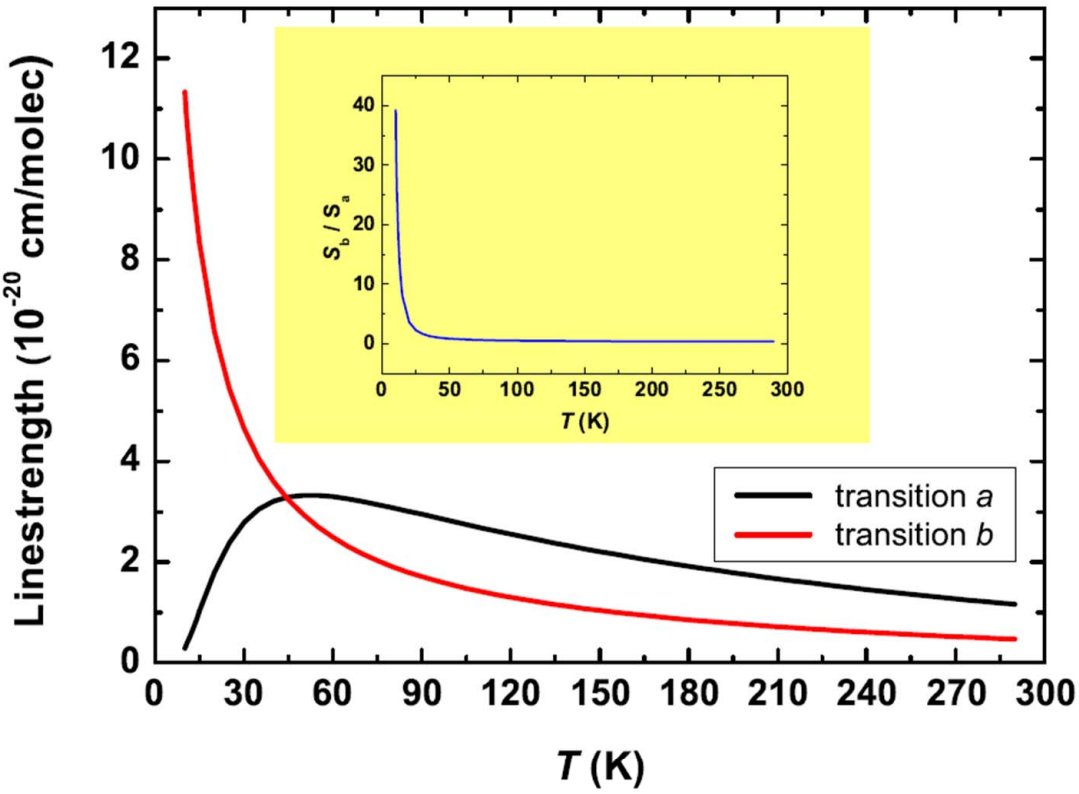

Figure 2.3: Linestrengths of a and b transitions, calculated using Eq. 2.2, are plotted as functions of rotational temperature. The ratio between the two curves is plotted in the inset.

in a subsystem-reservoir relaxation process have been both mathematically and physically established [Andersen et al. 1964]. To address this issue in our case, a normalized linestrength was measured for several ro-vibrational lines at a given translational temperature. The acquired behavior was then compared with the theoretical line dictated by the Boltzmann law. In practice, as shown in Fig. 2.4, the ratio $R(E_f,T) \equiv S(E_f,T)/S(E_f,T_{ref}) = \int \delta(E_f,T,\nu)\,d\nu / \int \delta(E_f,T_{ref},\nu)\,d\nu$ was determined against E_f (i.e., for each of the transitions listed in Table 2.1) in correspondence with two different T_{trans} values, 19 and 28 K. It is worth pointing out that the normalization of $S(E_f,T)$ to $S(E_f,T_{ref})$ was necessary in order to get rid of the unknown dependence of $S(T_{ref})$ on E_f. The obtained data points were then

fitted with the function

$$R(E_f, T) = H \exp\left[c_2 E_f \left(-\frac{1}{T} + \frac{1}{T_{ref}}\right)\right] \ , \tag{2.4}$$

with H a proportionality constant, T being the fitting parameter. The above equation is nothing but Eq. 2.2 with $\left[1 - \exp\left(\frac{-c_2\nu_0}{T}\right)\right]\left[1 - \exp\left(\frac{-c_2\nu_0}{T_{ref}}\right)\right]^{-1} \simeq 1$. The extracted rotational temperatures were $T = (27 \pm 2)$ K and $T = (42 \pm 3)$ K for measured translational temperatures $T_{trans} = (19 \pm 2)$ K and $T_{trans} = (28 \pm 2)$ K, respectively. In both cases, the fit correlation coefficient was $\chi = 0.98$, consistent with the hypothesis of canonical invariance.

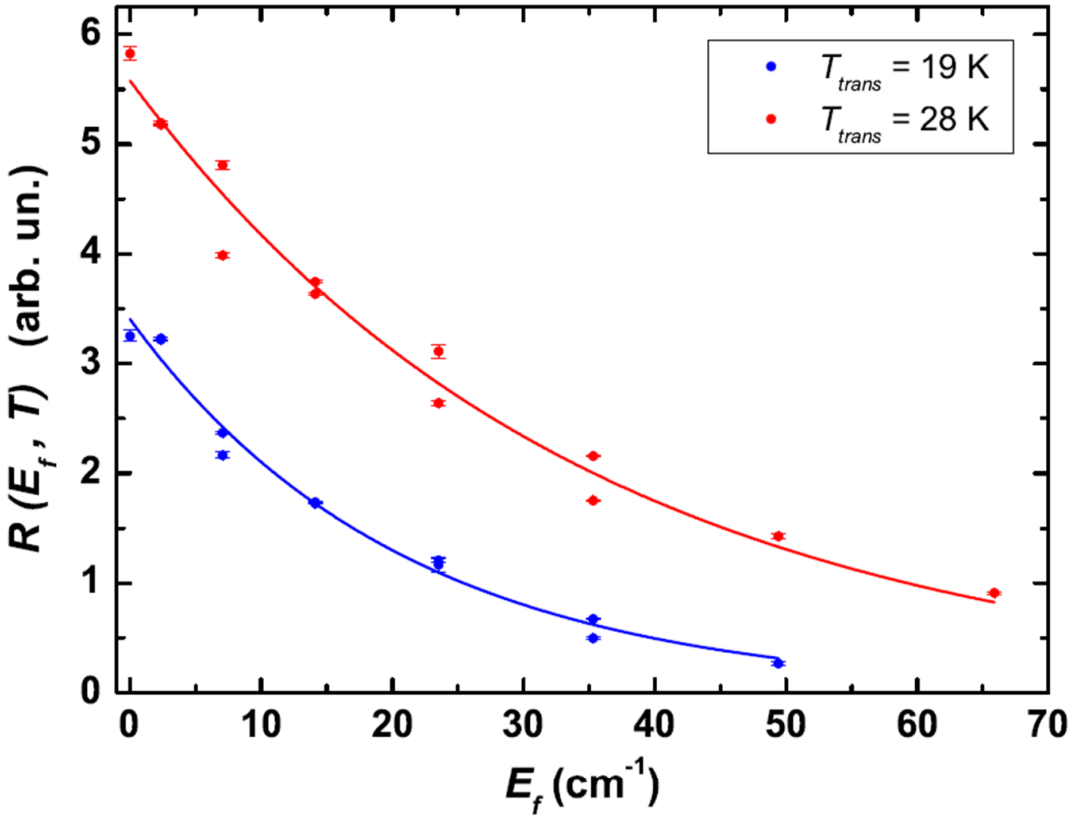

Figure 2.4: Ascertainment of the canonical-invariance hypothesis. Eq. 2.4 is fitted to the $R(E_f, T)$ data points measured as a function of the transition's lower-level energy for two different translational temperatures (19±2 and 28±2 K). The extracted rotational temperatures are 27 ± 2 and 42 ± 3 K, respectively, with a fit correlation coefficient of $\chi = 0.98$. Again, as in Fig. **??**, each data point is associated with a different pair of gas flows.

Table 2.1: Frequencies and lower-level energies of the ro-vibrational lines used throughout this work, as provided by the Hitran Database.

E_f (cm^{-1})	ν_0 (cm^{-1})	branch(J)
35.2979	6570.042687	R(5) $\equiv a$
23.5323	6567.844393	R(4)
14.1195	6565.620174	R(3)
7.0598	6563.370066	R(2)
2.3533	6561.094106	R(1) $\equiv b$
0	6558.792333	R(0)
2.3533	6554.111497	P(1)
7.0598	6551.732512	P(2)
14.1195	6549.327869	P(3)
23.5323	6546.897607	P(4)
35.2979	6544.441767	P(5)
49.4163	6541.960389	P(6)
65.8871	6539.453516	P(7)

2.3.3 Elastic cross section

Finally, by comparing the measured diffusion time of $^{12}C_2H_2$ in the BGC cell (vs the ^{4}He flux) with that predicted by a Monte Carlo simulation, we provided an estimate for the elastic cross section relevant to the translational cooling mechanism [Lu & Weinstein 2009, Skoff et al. 2011]. Let us start by looking a little more closely at the physics of the problem. After reaching thermal equilibrium with the He bath (under our typical experimental conditions, this happens on a path shorter than 100 μm, corresponding to about 50 collisions), a generic acetylene molecule experiences a random walk, scattered by helium atoms, until it freezes on the cell's walls or escapes through the exit hole (to form the molecular beam); in both cases, it stops contributing to the laser absorption. The larger the helium density, the higher the number of scattering events and the longer the acetylene average diffusion time, τ_{diff}.

This latter quantity was experimentally determined for transition a via the relationship

$$\tau_{diff}(T_{trans}) = \frac{L_c^3\, n_{C_2H_2}(T_{trans})}{f_{C_2H_2}} = \frac{L_c^3}{f_{C_2H_2}} \frac{\sigma_D(T_{trans}) \int \delta_a(\nu, T_{trans}) d\nu}{S_a(T)\, L_c} \ , \tag{2.5}$$

where the spectroscopic derivation of the acetylene density (based on the Lambert-Beer law) was also used [Maddaloni book]. Then, the $S_a(T)$ value corresponding to the measured $\sigma_D(T_{trans})$ was calculated by means of Eq. 2.2, with E_f, ν_0, and $S_a(T_{ref} = 294\ \mathrm{K}) = 1.13 \cdot 10^{-20}$ cm/molec taken from the Hitran Database, and $Q(T)$ provided by Amyay and coworkers [Amyay et al. 2011]. It should be noted that, in the above procedure, $T = T_{trans}$ was inevitably assumed. To fix that, curve a in Fig. 2.3 was used to estimate the extent to which the discrepancy between T and T_{trans} (as measured in Fig. **??**) affects the determination of $S_a(T)$; this is reflected in conservatively augmented error bars on the τ_{diff} data points.

The helium density was derived though the formula [Hutzler et al. 2012]

$$n_{\mathrm{He}} = \frac{4 f_{\mathrm{He}}}{\pi r_h^2 \langle v_{\mathrm{He}} \rangle} \ , \tag{2.6}$$

with $\langle v_{\mathrm{He}} \rangle = \sqrt{8 k_B T_{trans} \pi^{-1} m_{\mathrm{He}}^{-1}}$ being the mean thermal velocity of helium particles (m_{He} is the helium atom mass). According to the above procedure, two sets of τ_{diff} vs n_{He} were recorded, corresponding to translational temperatures of 100 and 25 K, respectively.

In a second stage, a theoretical simulation was carried out to reproduce the measured acetylene diffusion times. In particular, the $^4\mathrm{He}-^{12}\mathrm{C_2H_2}$ interaction was processed by a conventional Monte Carlo method, whereas the molecule free evolution was made to follow Newton's law. Firstly, for a given translational temperature, an acetylene molecule was injected into the buffer cell at time $t = 0$ with its three velocity components extracted randomly according to the corresponding Maxwell-Boltzmann distribution. Then, the probability $\mathcal{P}$ that an interaction occurs in the elementary

interval time δt was calculated considering the ^{4}He$-^{12}C_2H_2$ relative velocity (v_{rel}), n_{He}, and a trial cross section (σ_{tr}): $\mathcal{P} = n_{\mathrm{He}}\,\sigma_{tr}\,v_{rel}\,\delta t$. After that, a random number $\mathcal{N}$ (between 0 and 1) was generated: if $\mathcal{N} < \mathcal{P}$, then the atom-molecule impact was allowed to take place and new random velocity components were consequently extracted; otherwise, the molecule evolved freely for a successive time interval δt. These steps were iterated for successive δt intervals until the molecule reached one of the walls: the time τ spent in the cell before freezing was accordingly calculated. The whole procedure was then repeated for a thousand injected molecules, namely the minimum allowed number which doesn't affect the simulation result; averaging over all the computed τ values eventually yielded τ_{diff}. Depending on the values of f_{He}, T_{trans} and σ_{tr}, a different time interval δt was used in the simulation. Its value was kept between 1 and 10 ns, i.e. always small enough not to alter the simulation outcome. For each of the two translational temperatures, the above simulation was carried out as a function of n_{He}, searching for the optimal pair of σ_{tr} values which strictly delimits the experimental points from above and from below. The results are shown in Fig. 3.8. The elastic cross sections were estimated to be $\sigma_{el}(T_{trans} = 100\ \mathrm{K}) = (4 \pm 1) \cdot 10^{-20}\ \mathrm{m}^2$ and $\sigma_{el}(T_{trans} = 25\ \mathrm{K}) = (7 \pm 2) \cdot 10^{-20}\ \mathrm{m}^2$. From experimental data points, a sort of saturation behavior can be recognized for the diffusion time. This has been reported in several other papers for atoms or molecules diffusing in noble gas environment and primarily ascribed to the dependence of the initial molecular spatial distribution on the helium density; other possible sources are the presence of impurities in the buffer gas as well as the formation of dimers [Sushkov & Budker 2008], [Lu et al. 2008], [Skoff et al. 2011]. None of these mechanism can be readily included in theoretical simulations.

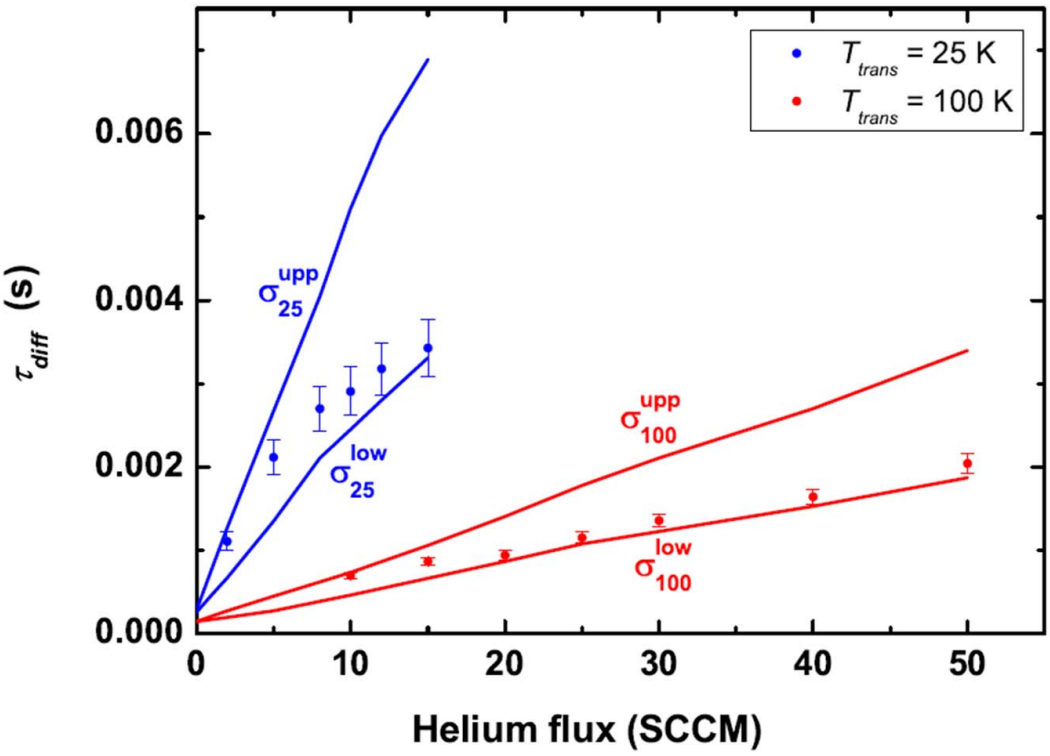

Figure 2.5: Experimental acetylene diffusion time plotted against f_{He} at a constant acetylene flux: $f_{\mathrm{C_2H_2}} = 5$ SCCM for $T_{trans} = 25$ K and $f_{\mathrm{C_2H_2}} = 50$ SCCM for $T_{trans} = 100$ K. Theoretical simulations (continuous lines) are also shown which delimit the measured data from above and from below ($\sigma^{upp}_{100} = 9.0 \cdot 10^{-20}$ m^2, $\sigma^{low}_{100} = 4.6 \cdot 10^{-20}$ m^2; $\sigma^{upp}_{25} = 4.9 \cdot 10^{-20}$ m^2, $\sigma^{low}_{25} = 3.1 \cdot 10^{-20}$ m^2), thus enabling the estimate of the total elastic cross sections.

Chapter 3

Comb-assisted cavity ring-down spectroscopy of a buffer-gas-cooled molecular beam

3.1 Introduction

By virtue of its applicability to nearly all species and its efficiency in producing very dense samples, the BGC method offers unique perspectives for low-temperature precision molecular spectroscopy. However, so far, only electronic molecular transitions have been addressed on BGC beams, either by laser-induced fluorescence (LIF) [Maxwell 2005, Stoll 2008, Yeo 2015, Barry 2011] or resonance-enhanced multi-photon ionization (REMPI) [Patterson 2009], whereas spectroscopy of the weaker but much narrower ro-vibrational transitions is still missing in the literature. In this thesis work, this gap is fill by demonstrating the applicability of a high-resolution and high-sensitivity detection technique, like cavity ring-down spectroscopy (CRDS), on a BGC molecular beam. At the same time, the current paradigm of comb-assisted absolute frequency metrology is also established. As an example, the performance of our scheme is evaluated for a 10-K C_2H_2 beam on the $g \rightarrow (\nu_1 + \nu_3)$ R(1) component

at 1.5-μm wavelength, yielding an uncertainty in the determination of the line-center frequency as low as 840 kHz.

3.2 Cavity ring down spectroscopy

The spectroscopic instrumentation generates a measurable signal that depends on the absorption of the target medium. Beer-Lamberts law expresses the fundamental behavior of laser absorption spectroscopy at a certain frequency ν : $I(\nu) = I_0(\nu)e^{-\alpha(\nu)L}$ where $I(\nu)$ and $I_0(\nu)$ are the intensities of the transmitted and incident laser light, respectively, $\alpha(\nu)$ is the medium absorption coefficient (cm^{-1}), and L is the effective optical pathlength (cm). Therefore, to obtain the optimum absorption sensitivity it is necessary to choose a strong molecular absorption line, use a platform with a long effective optical pathlength, and have a distinguishable absorption from baseline variations and laser power fluctuations.

The most important requirement is met by choosing a target line associated with fundamental absorption bands, as these are stronger than overtone or combination bands. A sufficiently long pathlength can be obtained by using multipass gas cells or cavity enhancement techniques. For sharp absorption lines, noise associated with laser power fluctuations can be reduced by averaging rapid scans over the time or by employing a modulation spectroscopy technique in the kHz regime. Cavity ring-down spectroscopy (CRDS), also known as cavity ring-down laser absorption spectroscopy (CRLAS), is a laser absorption technique, which takes advantage of the improved analytical sensitivity that is possible when making absorption measurements using extremely long path lengths.

CRDS relies on the fact that absorption is an additional loss in the cavity, and consequently changes its decay time, which is measured from the transient cavity transmission after an abrupt interruption of the injection [OKeefe et al. 1988, Romanini et al. 1997, Mazurenka et al. 2005, Lehmann et al. 1996].

The absorbance is then evaluated through a comparison between the decay time of the transmitted laser light, respectively, in the presence and absence of the gas sample. Alternatively, the comparison can be made between the decay time in correspondence of two wavelengths, on-and off-resonance.

While multiple longitudinal/transverse mode excitation, as realized when employing pulsed lasers, gives rise to multi-exponential decays (indeed each mode has its own characteristic ring-down time, RDT), excitation of a single cavity mode results, in principle, in a genuine single exponential process. Furthermore, use of pulsed lasers will more likely introduce unwanted interference effects in the light leaking out of the cavity, thus superimposing detrimental intensity modulations on the ring-down decay signal. As a result, the highest sensitivity will be achieved by use of a cw, narrow-linewidth laser.

The primary benefit of CRDS is that, in principle, it is not limited by the amplitude noise of the laser source, but only by the detection shot noise. In practice, however, drifts in the system between two consecutive measurements always prevent from achieving this ultimate limit and from averaging measurements over long times.

In the simplest scheme, the resonator length is continuously dithered by an annular piezoelectric actuator mounted on one of the cavity mirrors to bring the cavity mode frequencies into resonance with the laser beam. In this way, intensity will accumulate in the cavity (i.e., the cavity rings up); then, as a resonance builds up, a threshold detector triggers a large shift in the AOM frequency that rapidly brings the laser radiation out of resonance. If this switch-off is sufficiently fast (on the nanosecond timescale), a ring-down of the trapped light intensity will be recorded by a detector external to the cavity (obviously, the detector electrical bandwidth should be much greater than the inverse of the RDT). The average of many acquisitions, recorded by the oscilloscope, is then used to extract the RDT by means of a least-squares fitting routine; finally, hundreds of determinations of RDT yield the average cavity decay time together with its standard error.

When a fast laser pulse is transmitted into the ring-down cavity, it will gradually escape from the cavity as a small fraction of the light is transmitted through the mirrors at each reflection. A typical signal recorded by a detector placed at the exit mirror will behave as shown in Fig 3.1

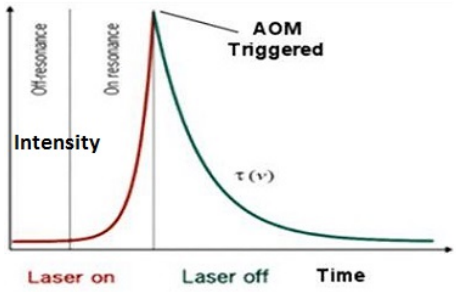

Figure 3.1: Schematic ring-down signals

Here each pulse corresponds to one cavity round trip by the laser pulse. The intensity I of light transmitted through the exit mirror will decrease as a function of time t according to the following exponential decay course

$$I(t) = I_0 e^{-\frac{t}{\tau}} \tag{3.1}$$

where I_0 is the initial detected light intensity and τ is the time it takes for the intensity to reach $1/e$ of I_0. The empty cavity ring down time τ is related to mirror separation d, mirror reflectivity R, and the speed of light c as follows:

$$\tau = \frac{d}{c \ln R} \tag{3.2}$$

In presence of a gas, the ring-down time will decrease because of of the additional decay process of absorption $e^{-\alpha ct}$ where α is the molecular absorption coefficient and the product of c and t, the absorption path length L. The exponential decay is now given by equation

$$I(t) = I_0 e^{-t/\tau - \alpha ct}. \tag{3.3}$$

The relationship between the empty cavity decay time τ and the decay time with an absorber present $\tau^{'}$ is then given by

$$\frac{1}{\tau^{'}} = \frac{1}{\tau} + c\alpha \tag{3.4}$$

By fitting the decay curve to an exponential and extracting $\tau^{'}$ from this fit is possible to determine the decay times and extract the α values in function of wavelength. Since CRDS measurements are independent of the initial source intensity, fluctuations from the source light doesnt limit sensitivity that is also increase thank to the long absorption path-lengths due to many laser round trips. However, the number of round trips, and therefore the path-length, is connected to the line strength of the absorbing species, for this reason the sensitivity is commonly expressed as the minimum detectable fractional absorption per laser round trip [Maddaloni book].

To obtain an expression for the limiting detection sensitivity consider a cavity of length L which is excited by a laser beam of intensity I_{in} ; then, after the first passage through the cavity, the intensity measured by the detector will be

$$I_0 = T^2 I_{in} e^{-\alpha d} \tag{3.5}$$

where T denotes the mirror intensity transmittivity, and the frequency-dependent absorption coefficient of a sample filling a region of length d inside the cavity. The factor $e^{-\alpha d}$ expresses the one-pass intensity attenuation due to absorption and/or scattering by the homogeneous sample, according to Lambert-Beer law. For each successive round-trip, the intensity diminishes by an additional factor of $R^2 e^{-2\alpha d}$, where R is the mirror intensity reflectivity so, after n round-trips, the intensity will be:

$$I_n = I_0 e^{-2n(lnR+\alpha d)} \tag{3.6}$$

Indicating with t = 2Ln/c, the time spent in the cavity by the light to travel the distance 2Ln, the intensity is $I(t) = I_0 e^{(-ct/L)(-lnR+\alpha d)}$ so the cavity ring down time is

$$\tau = \frac{L}{c(-lnR + \alpha d)} \simeq \frac{L}{c(1 - R + \alpha d)}. \tag{3.7}$$

This relation shows that the ring down time doesn't depend on the laser intensity and for this reason isn't affected by intensity. For an empty cavity the RDT is

$$\tau_0 = \frac{L}{c(1 - R)} \tag{3.8}$$

from which the mirror reflectivities can be accurately measured. Recording τ and τ_0 as functions of the laser frequency, the absorption spectrum of a sample within the cavity can be retrieved according to the following formula

$$\alpha(\nu) = \frac{L}{cd}(\frac{1}{\tau(\nu)} - \frac{1}{\tau_0}) \tag{3.9}$$

Finally, we can fix the limiting CRDS sensitivity as the minimum absorption coefficient, α_{min}, that can be detected in the limit of $\tau \longrightarrow \tau_0$

$$\alpha_{min} = \frac{L}{cd\tau_0}\frac{\Delta\tau_{min}}{\tau_0} = \frac{1 - R}{d}\frac{\Delta\tau_{min}}{\tau_0} \tag{3.10}$$

where $\Delta\tau_{min}$ is the minimum detectable change in the cavity ring-down time.

The last equation shows that the spectrometer sensitivity can be optimised either by increasing R or by increasing d, as well as by minimizing $\Delta\tau_{min}/\tau_0$ which represents the relative error of the cavity ring-down time measurements. Higher sensitivities can be reached by actively locking the cavity and laser in resonance, which originates higher and more reproducible intra-cavity intensities and therefore improved signals.

3.3 Frequency comb assisted laser spectroscopy

The field of precision spectroscopy has reached unprecedent developments thanks to a remarkable synergy between the technology of precision laser stabilization and mode-locked ultrafast lasers. This has resulted in a main control of the frequency spectrum with the advent of optical frequency comb synthesizers [Maddaloni 2009].

Mode-locked lasers generate short optical pulses by originating a fixed phase between all the longitudinal modes. In a time domain description, a mode-locked laser emits a train of pulses separated by the time $T = l_c/v_g$ where l_c is the length of the cavity and v_g is the net group velocity (Figure 3.2 a).

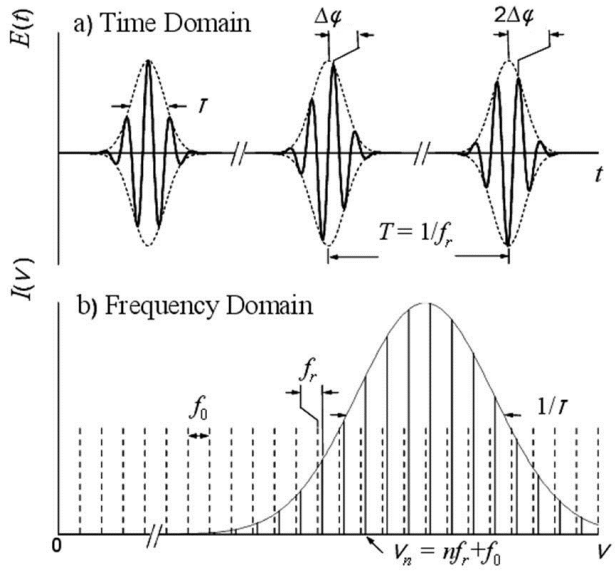

Figure 3.2: Consecutive pulses of the pulse train emitted by a mode locked laser and the corresponding spectrum

Due to dispersion in the cavity, the group and the phase velocity v_p are not equal, resulting in a phase shift of the carrier wave with respect to the peak of the envelope for each roundtrip, given by

$$\triangle \Psi = (\frac{1}{v_g} - \frac{1}{v_p}) l_c \omega_c \tag{3.11}$$

where ω_c is the carrier frequency. By taking the Fourier transform of the emitted field at a fixed spatial location, a comb spectrum in the frequency domain is obtained (Figure 3.2 b). It consists of equidistant regularly spaced lines with a frequency given by

$$\nu_n = nf_r + f_0 \tag{3.12}$$

where f_r is the laser repetition rate and $f_0 = \Delta\Psi f_r/2\pi$ represents an offset frequency.

In order to obtain a stable emission with absolutely known frequency, lasers can be locked to a self-referenced OFC synthesizer. The OFC synthesizer used in this experiment is based on an amplified mode-locked Er:doped fibre laser, followed by a nonlinear photonic fibre which generates an octave-spanning (between $1 - 2\mu m$) frequency comb of 250-MHz-spaced modes corresponding to the laser repetition rate f_r. Repetition rate and offset frequency are stabilized against a 10 MHz BVA quartz, locked to a Rb-clock, referenced to the Cs primary standard via global positioning system.

3.4 Experimental set-up

The experimental setup (Figure 3.3) consists of two main blocks: the BGC source and the laser spectrometer. Described in detail in chapter 2 of this thesis [Santamaria 2015], the heart of the BGC machine is represented by a cryocooler (Cryomech, PT415) housed in a stainless-steel vacuum chamber and fed with liquid helium by a compressor.

As a result of the BGC process followed by the expansion through the cell orifice, an acetylene beam at temperature T is created along the z direction with a mean longitudinal speed governed by the Reynolds number, Rey. In our case, this can be

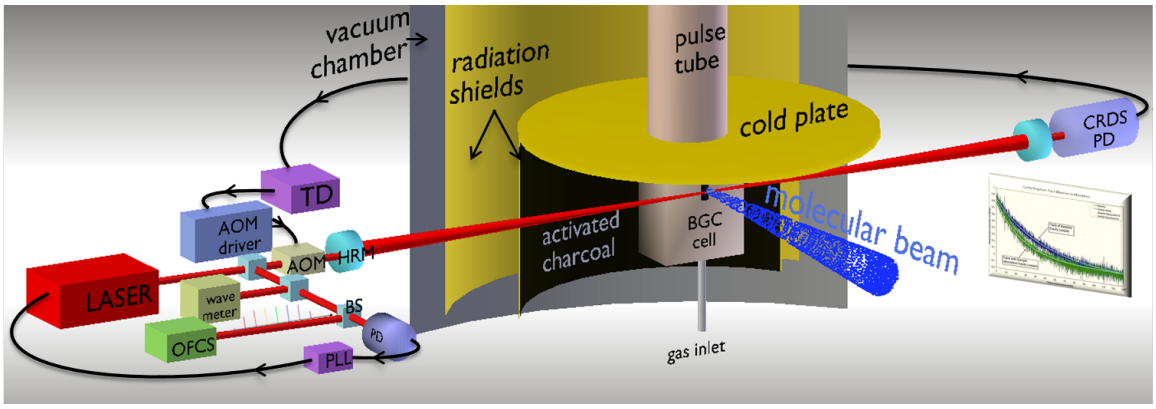

Figure 3.3: Layout of the experimental setup consisting of two main blocks: the buffer-gas-cooling source and the comb-referenced laser spectrometer. The following legend holds: HRM=high-reflectivity mirror, TD=threshold detector, PD=photo-detector, PLL=phase locked loop, BS=beam splitter.

expressed as [Hutzler 2012]

$$Rey \simeq \frac{4\, f_{\mathrm{He}}\, \sigma_{\mathrm{He-He}}}{a_x} \sqrt{\frac{\pi\, m_{\mathrm{He}}}{k_B\, T}}\,, \tag{3.13}$$

where m_{He} is the He mass and $\sigma_{\mathrm{He-He}} \simeq 3 \cdot 10^{-19}$ m^2 the elastic cross section for cold He collisions [Santamaria 2014]. For $T \simeq 10$ K and $f_{\mathrm{He}} < 15$ sccm, $Rey \leq 100$ is found, which allows to estimate the mean longitudinal speed as [Hutzler 2012]

$$\overline{v}_z \simeq 1.4 \sqrt{\frac{8 k_B T}{\pi m_{\mathrm{He}}}} \sqrt{1 - 4\, Rey^{-4/5}}\,. \tag{3.14}$$

Concerning the spectrometer, the laser source is a continuous-wave (CW) external-cavity diode laser delivering about 30 mW of power between 1470 and 1570 nm with a free-running emission linewidth less than 50 kHz at 5 μs (TopticaPhotonics, DLC CTL 1520). The laser output beam is split into three main parts (Figure 3.4). A part is sent to a wavelength meter with an accuracy of 0.2 ppm. Another portion is beaten against the Nth tooth of an optical frequency comb synthesizer (OFCS) of MenloSystems, FC-1500-250-WG (Figure 3.5) to provide a note at frequency ν_{beat}.

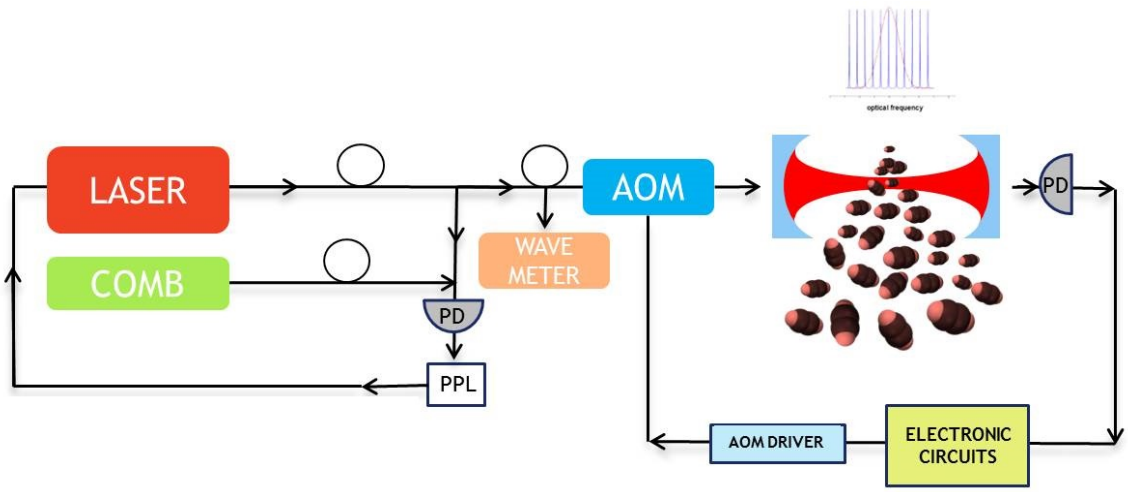

Figure 3.4: The laser output beam is split into three parts: one is sent with the OFC on a diffractive grating in superposition with the nearest COMB teeth to lock the laser through a PLL circuit; another part is sent to a wavelength meter; the last one is sent in the buffer gas apparatus trought an acusto-optical modulator (AOM) for the cavity ring down spectroscopy (CRDS) and is eventually collected by an InGaAs photo-detector (PD).

This latter is phase-locked by a dedicated electronic servo to a given local oscillator value ($\nu_{\mathrm{LO}} = 30$ MHz) by feeding back proper corrections to the laser external-cavity piezo transducer. The last portion passes through a fiber acousto-optic modulator (AOM) whose first-diffracted order is eventually injected into the high-finesse cavity. In this way, the laser emission frequency is determined as [Maddaloni 2009]

$$\nu_{\mathrm{laser}} = \nu_{\mathrm{ceo}} + N\nu_r + \nu_{\mathrm{beat}} + \nu_{\mathrm{AOM}} \tag{3.15}$$

where ν_{AOM} (80 MHz) is the frequency of the signal driving the AOM, while ν_{ceo} (20 MHz) and ν_r (250 MHz) denote the comb carrier-envelope offset and mode spacing, respectively. The link to the Cs-clock standard is established by stabilizing both ν_{ceo} and ν_r against a high-quality 10-MHz quartz oscillator which is disciplined, in turn, by a Rb/GPS clock; the same reference chain is used to lock the time base of the frequency synthesizers generating the signals at ν_{LO} and ν_{AOM}, respectively. Finally,

Figure 3.5: Optical frequency comb synthesizer controll of MenloSystems

the integer N is determined, through Eq. (3.15), by measuring the laser frequency with a 0.2-ppm-accuracy wavelength meter. In this way, the absolute frequency of the laser radiation can be monitored by simultaneously counting the frequencies ν_{ceo}, ν_r and ν_{beat} in Eq. (3.15). Then, tuning of ν_{laser} across the molecular resonance is accomplished by varying ν_r in discrete steps (at a given N). For each ν_{laser} value, the acetylene absorption is recorded according to a CW CRDS scheme [Romanini]. For this purpose, the laser beam is coupled to an enhancement optical resonator consisting of two facing high-reflectivity spherical mirrors (3 m radius of curvature, 1 inch diameter) at a distance of $D = 65$ cm along the x axis. Each mirror is held within the mount against a large-diameter o-ring, which permits angular adjustment of the mirror while maintaining a gas seal; a brass backing ring fits onto the back surface of the mirror, providing a contact point for the ball tips of the alignment screws. Two HR mirrors were bought from Los Gatos Inc. and one of them is showed in

Figure 3.6. The resonator length is continuously dithered by an annular piezoelectric actuator mounted on the input mirror.

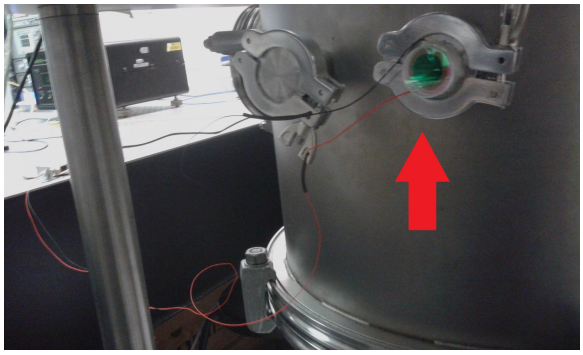

Figure 3.6: CRD mirror

3.5 Measurements

As a resonance builds up, a threshold detector switches the AOM off; the subsequent ring-down decay is detected by a transimpedence amplified InGaAs photodetector (5 MHz electrical bandwidth). The average of 50 acquisitions, recorded by the oscilloscope, is then used to extract τ by means of a LABVIEW® least-squares fitting routine [Maddaloni 2010]. In the presence of a molecular resonance, the absorption coefficient $\alpha(\nu)$ is then recovered through the relation [Berden 2000]

$$\alpha(\nu, z) = \frac{1}{c}\left[\frac{1}{\tau(\nu)} - \frac{1}{\tau_e}\right]\frac{D}{d_x(z)} \equiv \alpha'(\nu)\,\frac{D}{d_x(z)}\,, \tag{3.16}$$

where $d_x(z)$ is the molecular beam diameter along the x axis (i.e. the laser propagation direction) at the z coordinate, c the speed of light, and $\tau_e \simeq 10$ μs the empty-cavity decay constant corresponding to a finesse $\mathcal{F} = (\pi\, c\, \tau_e)/D \simeq 14000$.

Doppler broadening is the dominant line broadening mechanism in the beam so the observed absorption profile, $\alpha'(\nu)$, is then fitted by a Gaussian distribution

$$G(\nu) = G_0 \exp\left[-\frac{4\ln 2\,(\nu-\nu_0)^2}{w^2}\right]\,, \tag{3.17}$$

where the amplitude G_0, the transition center frequency ν_0, and the Doppler width

$$w = \frac{\nu_0}{c}\sqrt{\frac{8\ln 2\, k_B T}{m}}\,, \tag{3.18}$$

represent the fitting parameters, with m denoting the molecular mass. Subsequently, the temperature of the molecular beam, T, is obtained through Eq. (3.18).

Fig 3.7 shows the CRDS absorption signal at a distance $z_1 = 1$ cm from the BGC cell exit, obtained for $f_{C_2H_2} = 5$ sccm and $f_{He} = 10$ sccm. In these conditions, the temperature measured for the C_2H_2 beam is $T = (13.2 \pm 0.5)$ K, corresponding to $Rey \simeq 60$ and hence to $\overline{v}_z \simeq 340$ m/s. The center frequency of the $(\nu_1 + \nu_3)$ R(1) ro-vibrational line is measured as $\nu_0 = (196\,696\,652.0 \pm 0.8)$ MHz.

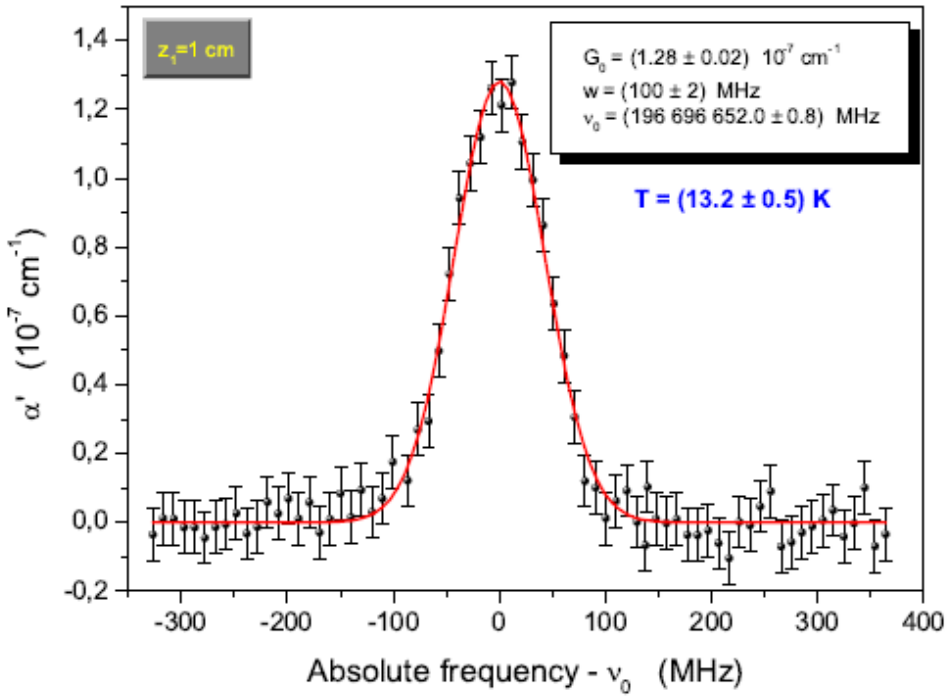

Figure 3.7: CRDS signal, with a signal-to-noise ratio of SNR $\simeq 30$, corresponding to $f_{C_2H_2} = 5$ sccm and $f_{He} = 10$ sccm, as measured on the acetylene beam at a distance of $z_1 = 1$ cm from the exit slit of the BGC cell. The center frequency of the $(\nu_1 + \nu_3)$ R(1) ro-vibrational line is measured with a fractional accuracy of $4.1 \cdot 10^{-9}$.

From this signal, the angular divergence of the molecular beam can also be estimated as follows. The starting point is to simulate the trajectories of the molecules escaping from the BGC cell, in order to reconstruct the beam shape at z_1. To this aim, a biased Maxwell-Boltzmann velocity distribution with uniform spatial density is first assumed on the exit slit ($z = 0$),

$$n_{MB}(v_x, v_y, v_z) \propto \exp\left[-\frac{m\, v_x^2}{2k_B T}\right] \cdot \exp\left[-\frac{m\, v_y^2}{2k_B T}\right] \cdot \exp\left[-\frac{m\,(v_z - \overline{v}_z)^2}{2k_B T}\right] . \qquad (3.19)$$

Afterwards, a single molecule is extracted with random velocity (within n_{MB}) and position, (within the exit slit rectangle) and made to follow a rectilinear trajectory with these initial conditions; its position is then calculated as a function of the z coordinate. This procedure is repeated for a huge number ($\sim 10^5$) of particles, which allows to retrieve the transverse profile of the molecular beam along z (see Fig. 3.8). This yields, in particular, $d_x(z_1) \simeq 0.2$ cm (root mean square), corresponding to a full angular divergence of $\Delta\phi = 2 \cdot \arctan[d_x(z_1)/z_1] \simeq 23°$.

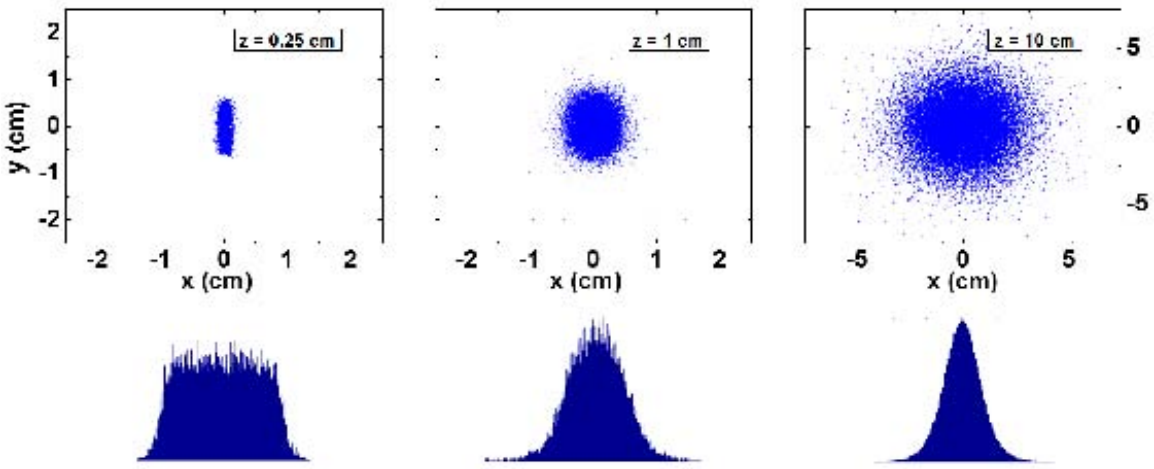

Figure 3.8: Simulation of the transverse profile of the molecular beam at different positions along the z axis, carried out for $\overline{v}_z = 340$m/s and $T = 13.2$K.

Then, we can calculate the average molecular density (along x) at z_1, $\overline{n}(z_1)$, using the following formula,

$$\overline{n}(z_1)\,\frac{S}{w} \simeq \alpha(\nu_0, z_1) = \alpha'(\nu_0)\,\frac{D}{d_x(z_1)}\,, \tag{3.20}$$

where $S \simeq 0.9 \cdot 10^{-19}$ cm/molec is the linestrength of the $(\nu_1 + \nu_3)$ R(1) ro-vibrational line at $T \simeq 13.2$ K [Santamaria 2015] and $w \simeq 100$ MHz is the Doppler width extracted by the fit. Finally, with reference to Fig. 3.9, from $\overline{n}(z_1) \simeq 1.6 \cdot 10^{12}$ molec/cm^3 and denoting with $\rho \simeq 670$ μm the laser beam waist in the high-finesse cavity, we estimate the molecular beam flux as $\mathcal{Z} \simeq \overline{n}(z_1)\,\overline{v}_z\,\rho\,d_x(z_1) \simeq 7.1 \cdot 10^{14}$ molec/s.

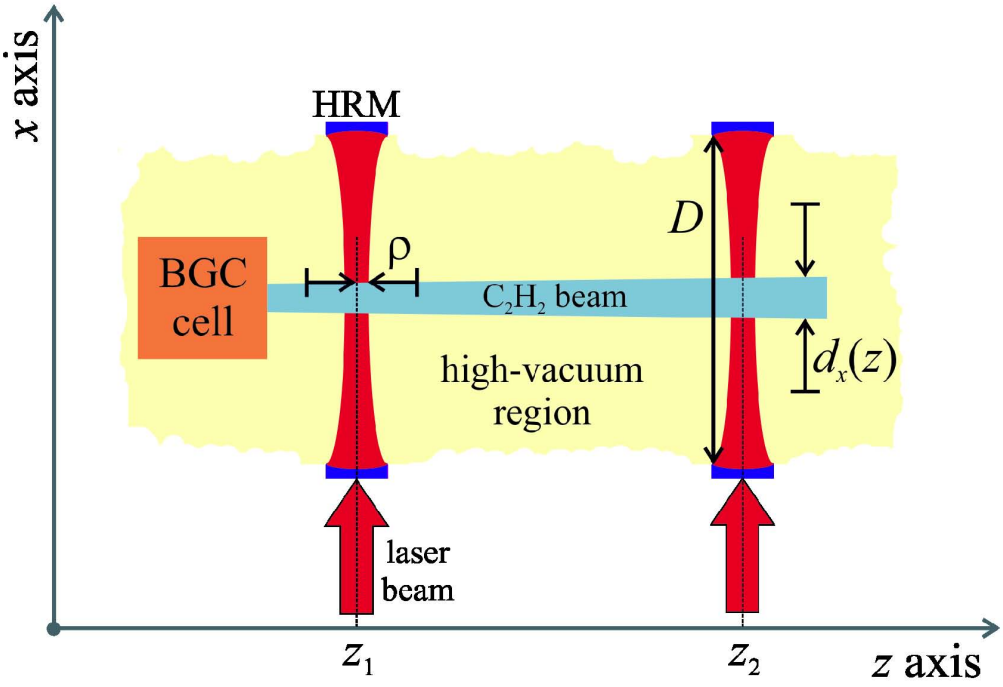

Figure 3.9: Schematic topview (not to scale) of the CRDS setup evidencing the relevant geometrical parameters involved in the estimation of the molecular beam density and divergence.

To test the validity of our spectroscopic approach at greater distances from the BGC source, the cavity ring-down signal is also measured at $z_2 = 10$ cm for the

same ro-vibrational transition, as shown in Fig. 3.10. In this case, higher flux values are used ($f_{C_2H_2} = 40$ sccm and $f_{He} = 10$ sccm) to obtain a signal-to-noise ratio of SNR $\simeq 7$. This bodes well for future implementation of more refined schemes to suppress transit-time broadening, such as Ramsey's method of separated fields in the optical domain [Constantin 1999], provided that both the molecular beam figures and the laser spectrometer performance are substantially improved. Indeed, much room for progress can come from optimization of the injection of $f_{C_2H_2}$ and f_{He} as well as of the geometrical parameters of the BGC cell in order to increase the output beam flux, while reducing its temperature and divergence. On the other side, we can work towards a more robust cavity design, also including superior-quality mirrors, as well as for a probe laser source with higher spectral purity. Ultimately, the spectroscopic measurement accuracy may enormously be enhanced by using an ultra accurate and stable microwave or optical frequency standard, as delivered by an actively stabilized optical fiber link [Calonico 2014].

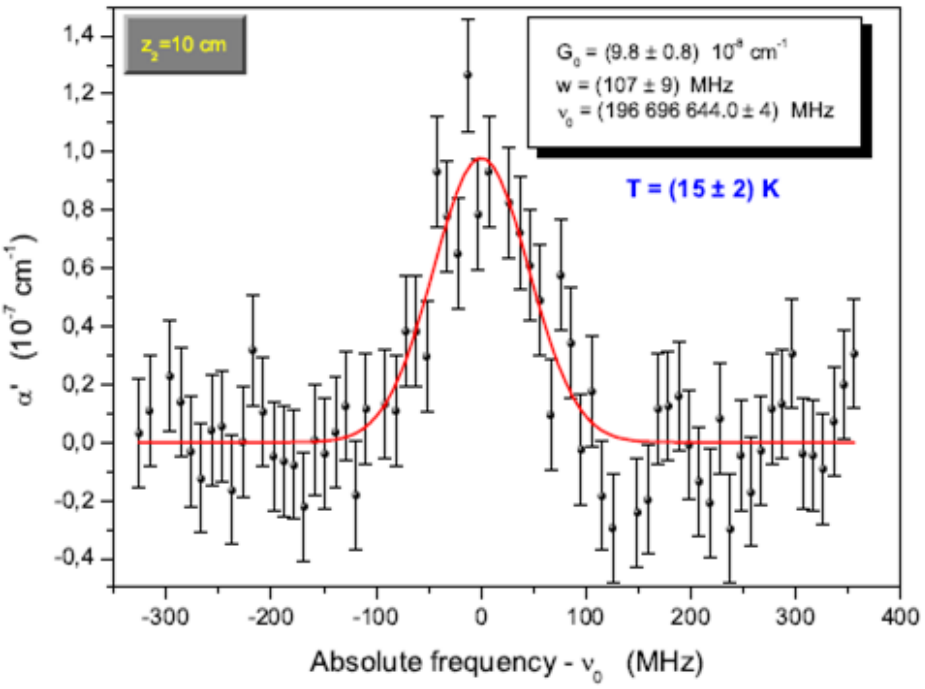

Figure 3.10: CRDS signal measured (for the same ro-vibrational transition) on the acetylene beam at a distance $z_2 = 10$ cm from the exit slit of the BGC cell. Here, higher flux values are used ($f_{C_2H_2} = 40$ sccm and $f_{He} = 10$ sccm), leading to a slightly increased beam temperature, $T = (15 \pm 2)$ K, and a larger Reynolds number, $Rey \simeq 220$. This corresponds to a beam longitudinal speed $\overline{v}_z \simeq 1.4\sqrt{\frac{8k_BT}{\pi m_{He}}} = 390$ m/s [Hutzler 2012].

Chapter 4

Future prospects: Assessing the time constancy of the proton-to-electron mass ratio by precision ro-vibrational spectroscopy of cold molecules

4.1 Introduction

Thanks to the tremendous progress experienced during the last decades in the field of atomic, molecular and optical (AMO) physics, the common paradigm according to which very high energies are essential to produce and detect exotic particles associated with physics beyond the Standard Model is being overcome in an increasing number of laboratories around the world [Orzel 2012]. Indeed, basically relying on the breakthrough technologies originated respectively from the world of ultracold quantum gases and that of femtosecond laser frequency combs, methods of precision spectroscopy have advanced to the point where atomic/molecular transition

frequencies can be determined with an astonishing accuracy (up to the level of a few parts in 10^{18}), to such an extent that detecting the influence of fundamental new physics at the eV energy scale is now within reach. In this frame, more and more challenging experiments are underway, aiming at testing nature symmetries and constants with unprecedented sensitivity. In particular, in the last few years there has been a strong interest in the possibility that what we know as the fundamental physical constants might show variations over cosmological time scales, such an effect arising quite naturally in modern theories attempting to unify gravity and other interactions [Uzan 2003].

Settling into this debate, the main goal of our proposed research is to constrain over a-few-years timescale the fractional temporal variation of the proton-to-electron mass ratio, $\beta = m_p/m_e$, at a level of 10^{-15}/yr by means of a spectroscopic frequency measurement on a sample of cold stable molecules, hinging on a refined Ramsey-fringes interrogation scheme. At the heart of the experiment will be the generation of a decelerated beam of cold molecules according to the novel techniques for direct cooling of ground-state molecules as opposed to the creation of dimers via magneto/photo-association of ultracold alkali atoms. The spectroscopic probe source will be based on a mid-infrared quantum cascade laser phase-locked to an *ad-hoc*-developed optical frequency comb (OFC), ultimately referenced to the Cs primary standard.

4.2 An Introduction to variability of the proton-to-electron mass ratio

Although it may seem like a bizarre supposition, the first conjecture on the temporal variation of fundamental constants dates back to Dirac's big-numbers hypothesis, which suggested in particular that Newton's gravitational constant decreased with the inverse of time [Dirac 1937]. On the other hand, generalized Kaluza-Klein models [Marciano 2004] and more recent string theories [Kiefer 2004], in the effort

to incorporate gravitational physics into the Standard Model (SM), postulate the existence of additional compactified dimensions where a "fundamental" Lagrangian, containing the "true" constants of nature, can be defined for elementary objects (leptons, quarks and gauge bosons) [Karshenboim 2002]. Accordingly, since the size of these extra dimensions is well below the smallest distance explored so far with particle accelerators (10^{-16} cm), maybe on the order of the Planck length, $l_P = \sqrt{\hbar G/c^3} \sim 10^{-33}$ cm, contemporary physics is just studying the "low-energy" limit of the "true" Lagrangian. In other words, everyday world is described in terms of factual parameters, that are effective coupling constants (CCs) and particle properties (PPs), which enter the actual Lagrangians corresponding to the four known fundamental interactions. In this picture, it's the extent of the extra dimensions to ultimately determine, through these factual parameters, the strength of forces in 4-dimensional (4D) world. Then, space-time changes in the strength of known interactions are predicted as a direct result of the cosmological evolution of the extra-dimensional subspace; such a circumstance would manifest itself as a variance of the effective CCs and PPs (electric charge, mass, magnetic moment). Also, in several theories (e.g. Superstrings), such variations result from the cosmological evolution of the vacuum state (a vacuum condensate of some scalar field or *Quintessence*) [Ivanchik 2003]. From an experimental perspective, it is most practical to search for variation of dimensionless quantities. The fine structure constant, $\alpha = e^2/(4\pi\varepsilon_0\hbar c)$, determining the strength of the electro-weak interaction, is the prime target of modern research in this area. In quantum chromodynamics (QCD), a similar coupling constant, α_s, exists for the strong interaction. However, since this latter is highly nonlinear, α_s is not well defined. Rather, the strength of the strong interaction is characterized by the parameter $\Lambda_{QCD} = 214^{+38}_{-35}$ MeV, which is defined as the position of the Landau pole in the logarithm for the strong coupling constant, $\alpha_s(r) = C/\ln[r\Lambda_{QCD}/(\hbar c)]$, where C is a constant and r the distance between two interacting particles [Chin 2009]. Since most of the proton mass stems from the gluon particle field surrounding the quarks, rather than from the quarks themselves, QCD basically predicts that $m_p \propto \Lambda_{QCD}$.

Thus, the second prominent dimensionless quantity is the proton-to-electron mass ratio, $\beta = m_p/m_e$, which characterizes the strength of strong interactions in terms of the electro-weak. At present, NIST lists the following values of these constants: $\alpha^{-1} = 137.035999074(44)$ and $\beta = 1836.15267245(75)$ [Mohr 2012].

At this point, it is worth acknowledging that the expansion of the Universe may have led in past, and still lead, some specific time and space changes which are similar to a variation of "constants". An illustration can be found in the widely credited Inflation model of the Universe according to which, at a very early stage of evolution, a phase transition caused by cooling of the Universe as a result of expansion drastically changed several properties of elementary particles, especially the electron and the photon [Borner 2004]. Indeed, the Standard Model of evolution suggests that a change of the electron mass from zero to some nonvanishing value, m_e, eventually arose from cooling of matter; this was also a phase transition for its electric charge e. The proton mass, instead, remained essentially the same. Indeed, it is deemed that only the masses of the naked quarks (so-called current quarks), essentially responsible for the small difference between the proton and the neutron mass, were changed during the phase transition caused by cooling of the Universe. But, to our current knowledge, Universe is still expanding and cooling and this should lead, as well, to some variation of m_e and e. Although these effects are tiny and not detectable now, they provide a clear indication that fundamental properties of basic particles, e.g. the charge and mass of the electron, should vary with time. The unanswered question of whether there is a reason for a faster variation, which is detectable with current experimental accuracy, is likely related to the outcome of the above multidimensional theories.

4.3 Research Program

As we will see shortly, while for the fine structure constant the temporal stability is effectively probed through atomic transitions [Lea 2007], this is not the case for the proton-to-electron mass ratio which is, instead, more accurately investigated

by means of molecular systems. Hence, the search for a possible time variation of β is currently focusing along two major directions. One route is to compare wavelengths of molecular lines as measured at present epoch on the Earth with the corresponding ones from astronomical objects at redshifts up to 3 (look-back time $\approx$ 12 Gyr) [Molaro 2010]. In this case, the main drawback is that astrophysical data are retrieved from uncontrolled environments and, indeed, results obtained so far are inconclusive and sometimes contradictory [Chiba 2011]. Deduced from the observation of radio-frequency transitions of methanol in the PKS1830-211 galaxy, the most updated constraint is $\Delta\beta/\beta = (0.0 \pm 1.0) \cdot 10^{-7}$ at redshift $z = 0.89$ (corresponding to a look-back time of 7 billion years) which, assuming a linear temporal variation, implies a fractional variation $\dot{\beta}/\beta$ on the order of $10^{-17}\cdot\mathrm{yr}^{-1}$, consistent with a null result [Bagdonaite 2013]. Conversely, the second approach relies on all-laboratory-based, precision molecular spectroscopy experiments which offer the obvious advantage to manipulate all the relevant parameters accurately and to investigate possible systematic effects in detail. Different schemes have been proposed in this frame, ranging from molecular fountains [**?**] to molecular ions confined in radio-frequency traps [Bakalov 2010].

Following the scheme originally implemented by C. Chardonnet with a traditional supersonic beam [Shelkovnikov 2008], our plan is to constrain the fractional temporal variation of the proton-to-electron mass ratio at a $10^{-15}\cdot\mathrm{yr}^{-1}$-level by measuring the frequency of a given molecular ro-vibrational transition relative to the clock hyperfine transition in the Cs electronic ground state: $(F = 4, m_F = 0) \leftrightarrow (F = 3, m_F = 0)$. According to Table 4.1, such frequencies scale respectively as [Karshenboim 2004]

$$\nu(\mathrm{S}) = K_{\mathrm{S}} \cdot \beta^{-1/2} \cdot Ry \tag{4.1}$$

$$\nu(\mathrm{Cs}) = K_{\mathrm{Cs}} \cdot \left(\frac{\mu_{\mathrm{Cs}}}{\mu_B}\right) \cdot \alpha^2 \cdot F_{\mathrm{Cs}}(\alpha) \cdot Ry \tag{4.2}$$

where S indicates for the moment a generic molecular species. Here, the Ks are proportionality constants, μ_{Cs} is the magnetic dipole of the Cs nucleus, μ_B the

Table 4.1: Functional dependence on the fundamental constants for transition frequencies related to different kinds of energy intervals. Ry stands for the Rydberg constant and μ denotes the nuclear magnetic moment. The nuclear mass is approximated by $A \cdot m_p$; higher vibrational levels involve a certain correction factor that depends on β which is not included.

	Transition	**Energy scaling**
Atomic	Gross structure	Ry
	Fine structure	$\alpha^2 Ry$
	Hyperfine structure	$\alpha^2(\mu/\mu_B)Ry$
Molecular	Electronic structure	Ry
	Vibrational structure	$\beta^{-1/2}Ry$
	Rotational structure	$\beta^{-1}Ry$
Relativistic corrections		Function of α

Bohr magneton, Ry the Rydberg constant, and $F_{\mathrm{Cs}}(\alpha)$ is a dimensionless function accounting for relativistic effects in Cs, where its dependence on α is the power of 0.83.

From these formulas the following relationship between our observable and β is derived

$$\frac{1}{\frac{\nu(\mathrm{S})}{\nu(\mathrm{Cs})}} \frac{\partial\left[\frac{\nu(\mathrm{S})}{\nu(\mathrm{Cs})}\right]}{\partial t} = -\frac{1}{2\beta}\frac{\partial\beta}{\partial t} - \frac{2.83}{\alpha}\frac{\partial\alpha}{\partial t} - \frac{1}{\frac{\mu_{\mathrm{Cs}}}{\mu_B}} \frac{\partial\left[\frac{\mu_{\mathrm{Cs}}}{\mu_B}\right]}{\partial t} \tag{4.3}$$

Based on a 6-year record of increasingly precise atomic clock frequency comparisons at NIST (Al^+ vs Hg^+, Hg^+ vs Cs, H vs Cs, Yb^+ vs Cs) a coupled constraint of $\dot{\alpha}/\alpha = (-1.6 \pm 2.3) \cdot 10^{-17}$ yr^{-1} and $d/dt[\ln(\mu_{\mathrm{Cs}}/\mu_B)] = (-1.9 \pm 4.0) \cdot 10^{-16}$ yr^{-1} was given [Lorini 2008]. In principle, by resorting to the Schmidt model, these limits could be used to extract, in an indirect way, a bound on the temporal drift of β, too [Lea 2007]. Unfortunately, the uncertainty of the calculation within such a model, which relates the magnetic moment of the nucleus to that of a single unpaired electron, is quite high (usually from 25% to 50%). Nevertheless, for the

purposes of a $10^{-15}\cdot\mathrm{yr}^{-1}$-level test, the above constraints can be applied to facilitate the interpretation of the spectroscopic frequency measurement by reducing, in fact, Equation 4.3 to

$$\frac{1}{\dfrac{\nu(\mathrm{S})}{\nu(\mathrm{Cs})}}\frac{\partial\left[\dfrac{\nu(\mathrm{S})}{\nu(\mathrm{Cs})}\right]}{\partial t} \simeq -\frac{1}{2\beta}\frac{\partial\beta}{\partial t} \tag{4.4}$$

On the other hand, in the frame of the Grand Unification Theory (GUT), [Calmet 2002] Calmet and Fritzsch have shown that $\beta^{-1}(\partial\beta/\partial t) = R_c\alpha^{-1}(\partial\alpha/\partial t)$, where R_c is a number between 20 and 40, its actual value depending on the GUT details [**?**]. In light of this, given the current constraint on $\dot{\alpha}/\alpha$, a possible fractional time variation of β is not expected to be less than several parts in 10^{-16}/yr, which is consistent with the formulation contained in Equation 4.4. Accordingly, a spectroscopic frequency measurement, carried out over a few-years period, directly translates into a model-free assessment of the stability of the proton-to-electron mass ratio. In order to achieve the claimed sensitivity for our test, the spectroscopic interrogation time, which sets the ultimate resolution achievable in the single measurement, must be greatly enhanced. For this purpose, a Ramsey-fringes scheme will be adopted [Ramsey 1950]. Here, a molecular beam is made to interact successively with two standing waves generated from a probe laser. In this configuration, the ultimate spectral resolution is proportional to the signal fringe periodicity P, given by the ratio of the mean longitudinal speed of the molecules in the beam, u, to the distance D between the two interaction zones: $P = u/(2D)$. In the optical domain, this method has to be associated with a sub-Doppler technique in order to avoid scrambling of the fringe pattern. In the case of two-photon spectroscopy, the most convenient configuration is just represented by the two-zone geometry. Here, each of the interaction tracts corresponds to a laser standing wave and the only experimental condition is that the relative phase between them is fixed. This is easily fulfilled by generating both standing waves inside a single folded Fabry-Perot (FP) enhancement cavity (finesse 1000) comprising four mirrors in a U configuration. In this case, the Ramsey fringes

will be superimposed on the broader two-photon signal arising from the absorption in one single zone. Since the attenuation in the side fringes is basically determined by the longitudinal velocity dispersion, a significant improvement in the fringe contrast, or signal-to-noise ratio (SNR), is expected when using a cold molecular beam at temperature T: $SNR \propto (\Delta u)^{-1} \propto 1/\sqrt{T}$. By virtue of the Boltzmann distribution law, the low temperature also increases the population in the bottom state of the molecular transition under investigation. In conclusion, a great enhancement in the final resolution is achieved (well beyond the molecular natural linewidth) if a beam of slow an cold molecules is used. For a better understanding, the description of the proposed experiment is divided into three sections, dealing respectively with the preparation of the molecular beam, the implementation of an ultra-high-precision spectrometer, and the actual procedure for the spectroscopic frequency measurement.

But first, let's spend a few words on the choice of the molecular species S. In light of what discussed so far, the fluoroform (CHF_3) molecule offers several distinct advantages:

- It exhibits a strong ro-vibrational band with a favorable two-photon transition at 8.63 micron where high-performance quantum cascade laser sources can be developed and technology is now mature for the realization of effective optical frequency combs;

- Due to a relatively high dipole moment (1.67 Debye), it is well-suited to manipulation through external electric fields;

- It also possesses a fundamental ro-vibrational band around 3 micron, where the high-power optical parametric oscillator (OPO) already operating at INO in Naples could be used for the future realization of dipole force potentials [Kuma 2009].

4.3.1 Creation of the cold, decelerated molecular beam

The aim of this stage is to generate a fluoroform beam with the following characteristics: intense flux, low temperature, reduced longitudinal speed, and fair collimation both in the coordinate and velocity space. This will be attained by combining in cascade a buffer-gas cooling source with a Stark decelerator.

BGC is a robust technique which operates with nearly all atoms and molecules [Hutzler 2012]. Cooling of the desired species S, CF_3H in our case, at initial temperature $T_S(0)$, takes place inside a cryogenic cell filled with He buffer gas at low temperature T_b and density n_{He}. The relevant parameters of the process are summarized in Fig. 4.1. After a characteristic number of collisions N_{coll}, the translational temperature $T_S(N_{coll}) = T_b + [T_S(0) - T_b]\exp[-N_{coll}/k]$ of S comes arbitrarily close to equilibrium with the buffer gas; here $k = (m_S+m_{He})^2/(2m_S m_{He})$, where m_S (m_{He}) is the mass of S (He). Rotational degrees of freedom are also cooled during these collisions. Hence, in conjunction with the formula for the mean free path, $\lambda_{S-b} = d^2\langle v_{0,b}\rangle/(4f_{0,b}\sigma_{S-b}\sqrt{m_S/m_b})$, the following condition on the cell length is found: $L > N_{coll}\cdot\lambda_{S-b}$. Then, a beam of S is formed by allowing both He and S particles to exit the cell into a high-vacuum environment via a small square hole of side d. Three different expansion regimes can be identified, governed by the so-called Reynolds number, defined as the ratio of inertial to viscous forces in a fluid flow: $Re = F_{inert}/F_{viscous} \approx 8\sqrt{2}f_{0,b}\sigma_{b-b}/(\langle v_{0,b}\rangle d)$. The $Re < 1$ ($Re > 100$) region corresponds to effusive (supersonic) beams; in the intermediate regime ($1 < Re < 100$), which is a prerogative of BGC sources, a partially hydrodynamic beam is obtained. This represents a successful synthesis between an effusive beam, with which it shares a reduced mean forward velocity $v_{\parallel,S}$, and a supersonic one, with which it shares a reduced temperature (i.e. spread around $v_{\parallel,S}$); moreover, it exhibits a lower angular divergence $\Delta\theta$. More in detail, the beam extraction process can be regarded as a competition between diffusion to the wall (random walk) and pump out. Thus, the extraction efficiency, η_{extr}, is maximized by increasing the ratio between

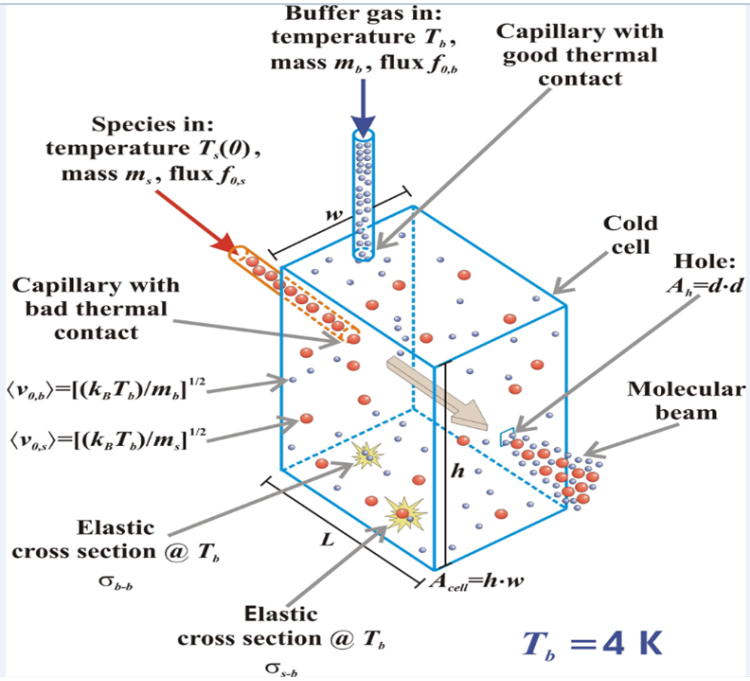

Buffer-Gas-Cell parameters for fluoroform (CHF_3)		
$f_{0,b} = 1$ SCCM	$d = 2$ mm	$Re = 5$
$f_{0,s} < 1$ SCCM	$h = w = 44$ mm	$\gamma \approx 0.1$
$T_s(0) = 298$ K	$L = 20$ mm	$v_{\parallel,s} = 69$ m/s
$N_{coll} \approx 75$	$\lambda_{s-b} = 0.08$ mm	$\Delta v_{\perp,s} = \Delta v_{\parallel,s} = 53$ m/s
$\sigma_{b-b} \approx 3 \cdot 10^{-19}$ m^2	$\langle v_{0,b}\rangle = 150$ m/s	$\Delta\theta = 21°$
$\sigma_{s-b} \approx 10^{-18}$ m^2	$\langle v_{0,s}\rangle = 36$ m/s	$\eta_{extr} = 1\%$

Figure 4.1: Relevant parameters of the buffer-gas-cooling process together with pertinent figures for a beam of fluoroform molecules.

the pertinent characteristic times, $\gamma \equiv \tau_{diff}/\tau_{pumpout} = \sigma_{S-b} f_{0,b}/(L\langle v_{0,b}\rangle)$, within the limits imposed by the partially hydrodynamic regime. In this case, a value close to 1% can be obtained for η_{extr}, with a velocity distribution similar to that inside the cell. For $Re = 5$, $v_{\parallel,S} = \langle v_{0,S}\rangle(1.2 + 0.6Re\sqrt{m_b/m_S}) \simeq 70$ m/s is found, while the velocity spreads are calculated as $\Delta v_{\parallel,S} \approx \Delta v_{\perp,S} \approx 1.5\langle v_{0,S}\rangle \approx 100$ m/s; this yields $\Delta\theta = 2\tan^{-1}(\Delta v_{\perp,S}/v_{\parallel,S}) \simeq 21°$. Also, on the basis of Monte Carlo simulations, with input fluxes of $f_{0,b} \simeq 1$ SCCM and $f_{0,S} < 1$ SCCM, a high output flux, $\mathcal{F}_S \approx 3 \cdot 10^{13}$ molec/s, is predicted. The divergence figure can be further improved by the use of

a skimmer which, however, inevitably reduces the beam flux; a good compromise is obtained for $\Delta\theta \simeq 2°$, corresponding to $\mathcal{F}'_S \simeq 6 \cdot 10^{11}$ molec/s. The beam region vacuum is maintained at 10^{-8} torr by a high-speed (3000 l/s) cryo-pump system based on activated charcoal; eventually, the buffer gas is rapidly pumped out. Soon under construction, the BGC setup will be based on a commercial two-stage pulse tube cryo-cooler.

After exiting the source cell, the CF_3H beam flies into a differentially-pumped intermediate cubicle and then comes into the utra-high-vacuum chamber (as guaranteed by use of an ionic pump) housing the Stark decelerator. It is worth pointing out that, at this stage, by virtue of the rotational cooling brought about by the BGC process, the population in the state $|J = 1, K = 1\rangle$, that is the lower rotational state in the selected two-photon transition, is enhanced by a factor of about 540 (compared to room temperature) up to 5%, thus yielding $\mathcal{F}''_S \simeq 3 \cdot 10^{10}$ molec/s. The SD acts on the created beam to dramatically reduce its longitudinal speed, while preserving the achieved temperature [Vandemeerakker 2012]. In order to realize the working principle of a Stark decelerator (SD), let us first recall that the behaviour of a neutral polar molecule (with dipole $\boldsymbol{\mu}$) in an external inhomogeneous electric field $\boldsymbol{E}$ is defined by the interaction energy $W = -\boldsymbol{\mu} \cdot \boldsymbol{E}$ and the associated force $\boldsymbol{F} = \nabla(\boldsymbol{\mu} \cdot \boldsymbol{E})$. In the adiabatic approximation, a local potential can be introduced, given by the molecular dipole times $|\boldsymbol{E}|$. In particular, in the presence of a minimum of $|\boldsymbol{E}|$, the so-called low-field-seeking (lfs) states (that are states whose energy increases with increasing electric field) experience a restoring force towards the minimum region. For a symmetric top molecule, like CF_3H, rotational states are labeled by three quantum numbers: J, the total angular momentum quantum number; K, describing the projection of the vector $\boldsymbol{J}$ onto the molecular axis; and M, representing the projection of $\boldsymbol{J}$ onto the local electric field vector. Among the different implementations, the most effective one is represented by the so-called traveling-wave Stark decelerator, where a suitable sequence of time-varying sinusoidal voltages, $V_n(t) = V_0 \sin[-\phi(t)+2\pi n/N]$, is applied to a longitudinal periodic arrangement of ring electrodes, where $N = 8$ is the array

periodicity (see Fig. 4.2). In this configuration, molecules in low-field-seeking (lfs) states experience a true 3D potential well that moves continuously along with them. Since one oscillation of the waveform moves the trap over one period, the velocity of the trap is given by $v_{trap}(t) = [L/(2\pi)] \cdot d\phi(t)/dt$, so that a constant deceleration is achieved by application of a parabolic phase (here, L denotes the periodic length that is the center-to-center separation between two consecutive rings times N). The main advantage of this kind of decelerator is that the molecules can be brought to a complete standstill and trapped without the need to load them into a separate electrode geometry. In the specific case of fluoroform, among the six $|J = 1, K = 1\rangle$ Stark substates, only two are low-field seeking: $|J = 1, K = 1, M = -1\rangle$ and $|J = 1, K = -1, M = 1\rangle$; therefore, assuming a lossless process (the so-called Majorana transitions are avoided by assuring that the electric field never drops below a certain minimum value), the beam flux emerging from the SD is reduced to $\mathcal{F}_S''' \simeq 1 \cdot 10^{10}$ molec/s. It should be mentioned that, since during free flight the molecular beam tends to spread out both in the transverse and longitudinal directions, additional electrodes are needed to re-focus the molecules through the different sections of the apparatus. For molecules in lfs states, transverse focusing can be achieved employing electrostatic hexapole lenses, while focusing in the forward direction can be accomplished using a buncher, both systems being just adaptions of the corresponding devices well-known in charged particle physics. In particular, the electric field in the buncher provides a harmonic focusing force along the beam direction, in the moving frame of the molecular beam; with such a device, both focusing in real space ("spatial focusing") and focusing in velocity space ("velocity focusing" or "longitudinal cooling") can be performed. In our proposed setup, an electrostatic lens is first needed to match the decelerator entrance; then, a system consisting of a number of hexapoles and bunchers is necessary to the transverse collimation as well as to the bunching of the slow beam emerging from the SD. By carefully designing the exact configuration of the whole arrangement of electrodes, and starting with a molecular beam longitudinal velocity of 70 m/s (as provided by

the BGC stage), a reduction down to 10 m/s should be affordable by use of the SD, while keeping a fine collimation along the entire distance required for the spectroscopic interrogation ($D = 0.5$ m). By summarizing, at the end of the cooling+deceleration

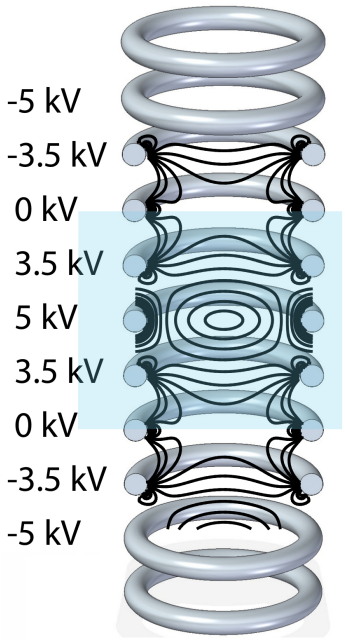

Figure 4.2: Sketch of the traveling-wave Stark decelerator. It consists of 336 ring tantalum electrodes, each of which is attached to one of eight stainless steel rods (where the sinusoidal voltages are appplied), resulting in a periodic array in which every ninth ring electrode is attached to the same rod.

process, the following characteristics should be available for the fluoroform beam on which to carry out the actual spectroscopic measurement:

- total flux in the lower rotational state of the selected two-photon transition: $\mathcal{F}_S''' \simeq 1 \cdot 10^{10}$ molec/s;
- mean forward velocity: $u = 10$ m/s;
- longitudinal, transverse and rotational temperature: $T = 4$ K;
- residual angular divergence: < 40 mrad.

Thus, the expected periodicity in the Ramsey-fringes signal is $P = u/(2D) = 10$ Hz.

4.3.2 Implementation of the ultra-high-resolution spectrometer

For the selected two-photon transition (see Fig. 4.3), ($\upsilon_5 = 0, J = 1, K = 1$) is the ground state, ($\upsilon_5 = 1, J = 2, K = 2, l = -1$) the intermediate level (here, l denotes the quantum number arising from the Coriolis coupling interaction), and ($\upsilon_5 = 2, J = 1, K = 1$) the excited state. Falling at 1158.83 cm^{-1} (the virtual level staying about 3.5 GHz below the intermediate one), it can be accessed by a distributed feed-back (DFB) QCL emitting around 8.63 micron. In order to measure the center frequency of such transition with the necessary resolution and accuracy, the realization of an OFC-referenced, ultra-stable and narrow probe source is needed. In the actual

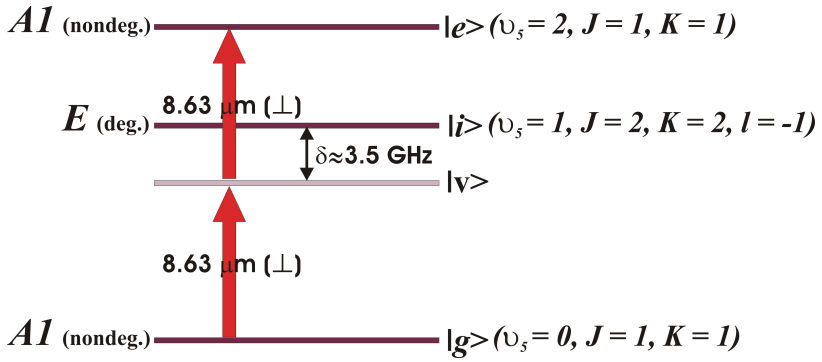

Figure 4.3: CF_3H two-photon transition selected for the Ramsey interrogation. The energy of rotational levels can be expressed as $E(J,K) = BJ(J+1) + (C-B)K^2 - D_J J^2(J+1)^2 - D_{JK} J(J+1)K^2 - D_K K^4 - 2\xi Kl$, with $B = 10.425$ GHz and $C = 5.716$ GHz being the leading constants.

setup (schematically shown in Fig. 4.4), a first laser (QCL1), previously locked against the resonance of an ultra-stable, high-finesse optical cavity, is referenced to an offset-free OFC, covering a 4-THz-wide interval centered at 8.63 micron. Expressly developed for this Project, the latter relies on an amplified Er:fiber oscillator whose output, spectrally broadened in an ultra-low-noise coherent way by use of specially designed fibers and integrated dispersion compensating devices, provides the input for an optimized difference-frequency-generation (DFG) process in a non-linear GaSe crystal. In particular, a sub-Hertz linewidth is reached for the comb teeth by upstream

stabilization against a high-performance, commercial optical reference system. The spectroscopic frequency measurement is then traced back to the Cs primary standard by stabilizing the mode spacing of the mid-infrared comb against the radio-frequency reference signal derived, via the National optical fiber link, from the fountain clocks (typical fractional frequency accuracy of $3 \cdot 10^{-16}$ and stability of $3 \cdot 10^{-14} \cdot \tau^{-1/2}$) operated at Istituto Nazionale di Ricerca Metrologica (INRIM). In such a scheme, referencing to the 8.63-micron OFC ensures that the QCL1 radiation has a stability of better than 1 Hz up to 1000 s, as required for data collection and averaging. Finally, a second laser (QCL2) is offset phase locked to QCL1 by means of a wide-bandwidth phase-locked loop (PLL), which makes QCL2 a replica of QCL1 in terms of spectral features, and used to excite the mentioned two-photon transition.

4.3.3 The actual spectroscopic measurement

In its last section, the deceleration chamber is equipped with a number of optical windows allowing for the propagation of the laser radiation which is tuned to the selected two-photon resonance. According to the Ramsey geometry described above, the molecular beam is made to interact successively with two standing waves (at a distance $D = 0.5$ m) generated starting from the QCL2 output beam (10 mW power). The input and output couplers of the U-shaped cavity are concave mirrors mounted on piezoelectric transducers in order to modulate or adjust the cavity length. The intermediate mirrors are flat with a 45° incidence. Reflection from the input mirror is used to lock the cavity to QCL2 through a Pound-Drever-Hall (PDH) technique, while fringes are detected on the transmission. Finally, the whole Ramsey cavity is surrounded by a μ-metal magnetic shield to avoid any fringe scrambling due to Zeeman effect. The central Ramsey fringes (several hyperfine components are expected to be resolved) are recorded by co-adding tens of frequency sweeps, alternating up and down, each of several seconds. Then, a suitable function is fitted to the obtained fringe pattern to yield the periodicity and the center frequency.

Regarding the latter, given the above figures for the probe laser and the molecular beam, and for a reasonable fringe contrast (SNR=50), the mean value of hundreds of individual measurements (about 500) should return a resolution (accuracy) of 0.05 Hz, corresponding to a fractional uncertainty of $1.5 \cdot 10^{-15}$. According to Eq. 4.4, this means that a comparison carried out over a few years would constrain the fractional temporal variation of the proton-to-electron mass ratio at the claimed level, provided that all the relevant systematic effects (second-order Doppler effect, ac Stark effect induced both by the blackbody radiation and the irradiated probe laser, collision shift, ...) are properly taken into account and subtracted. This would represent an order-of-magnitude improvement compared to present experiments. Indeed, so far, the most stringent (model-independent) test of the time-variation of β has been performed by comparing vibrational transitions in a supersonic SF_6 beam with a Cs fountain over 2 years, which has resulted in a limit of $5.6 \cdot 10^{-14} \cdot \mathrm{yr}^{-1}$ [Shelkovnikov 2008]. Finally, it is worth pointing out that the ultimate resolution (accuracy) in the frequency measurement might be greatly enhanced by stabilizing the frequency comb, to which the probe laser is referenced, against an optical atomic standard, like the Yb lattice clock already under construction at INRIM [Pizzocaro 2012]. In that case, a fractional frequency uncertainty as low as 10^{-18} could be reached.

4.4 Research Outcomes

The first immediate implication of this Project will be the opportunity to finalize over a-few-years timescale an ultra-sensitive, model-independent laboratory study of the temporal stability of the proton-to-electron mass ratio. As already mentioned, the entrance into such an intriguing matter is related to the possible validation of modern multidimensional theories beyond the Standard Model towards a Grand Unified Theory (GUT), which merges the three presently independent gauge interactions (electromagnetic, weak, and strong) into just one interaction (thus characterized by a single unified coupling constant). Indeed, while the observation of the new particles

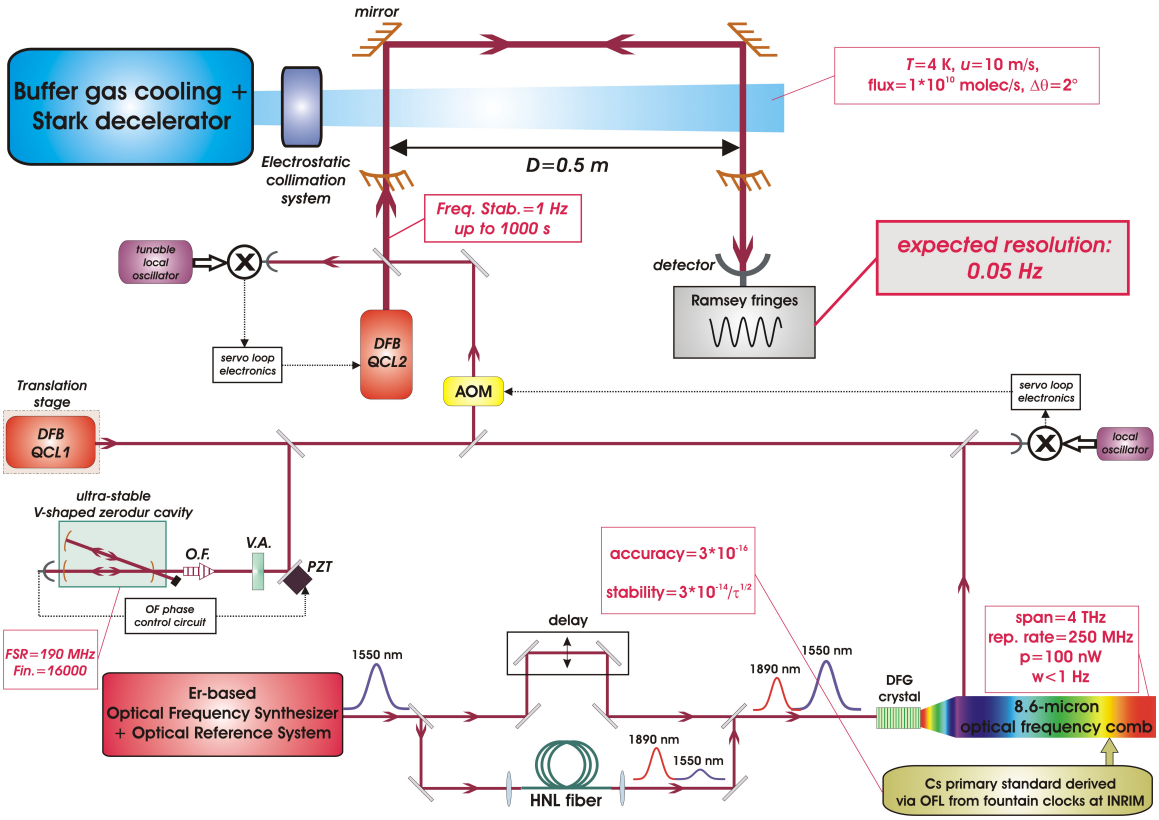

Figure 4.4: Schematic layout of whole experimental setup.

predicted by candidate GUTs (essentially based on Lie Groups) is far beyond the reach of currently foreseen collision experiments (the involved masses are expected to be a few orders of magnitude below the Planck scale) some predictions, like the time variation of fundamental constants, the existence of magnetic monopoles or electric dipole moments of elementary particles, might be addressed with precision spectroscopy of cold molecular samples [Fritzsch 2004]. Although not necessary, GUTs are often seen as an intermediate step towards a Theory of Everything (ToE), which reconciles the description of gravity and the large-scale structure of spacetime with the account of the small-scale structure of matter, presently entrusted to the General Relativity and the Standard Model, respectively. In this sense, ToE-aspirant theoretical frameworks (String/M-theories, Loop Quantum Gravity, . . .) [Kiefer 2004] would represent the long-awaited overcoming of these two main, successful but disjoint, physical frameworks. In this respect, it should be pointed out that, in such

theories, violation of the equivalence principle of General Relativity - the outcome of any non-gravitational experiment is independent of position and time - may occur and can be consistently described [Bethlem 2009].

4.4.1 Mid and long-term perspectives

Besides the prime repercussion, a large number of innovative research directions is expected to originate from the accomplishment of the proposed Research. Indeed, the availability of an effective source for cold and decelerated molecules in conjunction with the realization of an extremely sophisticated spectroscopic interrogation technique, like that based on the two-photon Ramsey fringes, will pave the way to high-sensitivity tests of a few other fundamental physics laws [Maddaloni 2013]. Among these, we mention, above all, the search for parity violation electroweak interactions through the detection of severely small ($\Delta\nu/\nu \sim 10^{-16}$) energy differences between different enantiomeric states of chiral molecules; to date no experiment has reached the resolution needed to observe this difference, but use of cold chiral molecules could improve these measurements [Darquie 2010].

Other applications are in the field of matter-wave interferometry, where quantum interference with very massive molecules, in the search for Schrödinger's cat, represents the most intriguing option.

4.4.2 More distant scientific horizons

More distant perspectives include secondary cooling strategies towards quantum degeneracy such as opto-electrical cooling or cavity-assisted laser cooling followed by evaporative or symphatetic cooling. In this frame, interacting with both the experimental and theoretical groups on ultracold atoms at European Laboratory for Nonlinear Spectroscopy (LENS) will be strategic. One can envisage that this trend of experiments, gradually approaching the quantum degeneracy regime, will take on and further expand the role of cold atomic physics and chemistry in the discovery of

new phenomena. In a successful scenario, the achievement of quantum degeneracy could pave the way to the exploitation of electric dipole-dipole interaction in optical lattices for the realization of new quantum computation platforms [Buchler 2007] or exotic quantum states [Micheli 2006].

Chapter 5

Conclusion

The emerging, powerful technologies for the cooling of stable molecules gives a new impetus to the molecular beam sources study [Carr et al. 2009]. Among the various schemes, at least for temperatures in the few-Kelvin range, the buffer-gas-cooling (BGC) method is perhaps the most efficient in terms of produced sample density and it is applicable to nearly all molecules [Maxwell et al. 2005, Bulleid et al. 2013]. Here, a noble gas, typically helium, is chilled just above its boiling point and acts as a thermal bath (buffer) that cools in turn, through collisions, the injected molecular gas under analysis.

Thanks to the implementation of a modern buffer-gas-cooling technique, the range of cryogenic temperatures for the spectroscopic study of acetylene in a helium environment is extended, with respect to previous literature, down to a few Kelvin. In order to accurately determine the achieved translational and rotational temperatures, several ro-vibrational transitions belonging to the $(\upsilon_1 + \upsilon_3)$ band were used for Doppler thermometry and measurements of relative intensities. A deeper insight into the collisional cooling process is gained by measuring the acetylene diffusion time in the buffer cell against the helium density at two temperatures that spanned a large range (100 and 25 K); in this respect, an appropriate theoretical model is also developed, which allowed us to obtain an estimate for the respective elastic

cross sections. These studies may be particularly useful in planetary science when modeling the process of translational energy relaxation of molecules in bath gases, which is crucial for understanding the energy balance of the upper atmosphere and its evolution [Bovino et al. 2011, Nan & Houston 1992]. While insignificant in the range of pressures explored in this work, pressure broadening and shifts are also of foremost importance at temperatures of astrophysical relevance and, as such, will be the subject of future investigations. Furthemore, by virtue of the enormous versatility of our buffer-gas-cooling apparatus, the spectroscopic study reported here may be readily extended to other fundamental atmospherical and astrophysical molecular species such as, for instance, methane [Onstott et al. 2006, Lellouch et al. 2009], nitrous oxide [Ziurys et al. 1994], and carbon dioxide [Oancea et al. 2012].

The potential of our set-up to tune the thermal equilibrium between translational and rotational degrees of freedom is also demonstrated. This can be used to reproduce in a controlled way the regime of non local thermal equilibrium typically encountered in the interstellar medium. The underlying helium-acetylene collisional physics is also addressed in this thesis. In particular, buffer gas cooling with a ^{4}He gas is used to perform laser-absorption spectroscopy of the $^{12}C_2H_2$ ($\nu_1 + \nu_3$) band at cryogenic temperatures. Doppler thermometry is first carried out to extract translational temperatures from the recorded spectra. Then, rotational temperatures down to 20 K are retrieved by fitting the Boltzmann distribution to the relative intensities of several ro-vibrational lines. The diffusion time of $^{12}C_2H_2$ in the buffer cell is measured against the ^{4}He flux at two separate translational temperatures; the observed behavior is then compared with that predicted by a Monte Carlo simulation, thus providing an estimate for the respective total elastic cross sections: $\sigma_{el}(100\text{ K}) = (4 \pm 1) \cdot 10^{-20}$ m^2 and $\sigma_{el}(25\text{ K}) = (7 \pm 2) \cdot 10^{-20}$ m^2.

However, accurate analysis of spectral lineshapes represents a powerful tool for probing fundamental atom-molecule low-temperature interaction processes; obtaining molecular spectra with enhanced signal-to-noise ratios is vital for addressing this issue with the implementation of a cavity ring-down spectroscopy technique. For this reason

a comb-assisted high-sensitivity spectroscopy of molecular buffer gas cooled beams is performed. From the experiment data, the average molecular beam density and the molecular beam flux at $T \simeq 13.2$ K are estimated. The cavity ring-down signal is also measured at greater distances from the BGC source to test the validity of this spectroscopic approach.

The effective and general CRDS technique reported here will immediately have a broad impact on the field of precision spectroscopy with molecular buffer-gas beams, being applicable to a wide range of additional species in different spectral regions. As an example, in the wake of traditional supersonic beams, our approach will enable a new generation of low-temperature, high-resolution ro-vibrational spectroscopic investigations on simple molecules of atmospheric or astrophysical interest, aimed at both fundamental physics studies and applications. Finally, other interesting variants, cavity-enhanced direct frequency comb spectroscopy [Adler 2010] above all, may be extended to buffer-gas cooled samples, too.

Could be intriguing the implementation of our set up for the meausurement of the temporal stability of the proton-to-electron mass ratio according to the Ramsey geometry described in the chapter 4. Here, the molecular beam will be made interrogated successively with two distant standing waves. Finally, could also be extremely interesting to explore the molecular beam properties in the epitaxy process during the thin film growth.

Within MBE system, the atoms or molecules in the gas deposit on the substrate to form the growing solid layer. Typically, each element is guided in a separately controlled beam, so the choice of elements and their relative concentrations can be adjusted for any given layer, defining the precise composition and electrical and optical characteristics of that layer. These materials are layered one on top of the other to form transistors, lasers and other semiconductor devices used, for example, in fiber-optics, cellular phones, satellites, radar systems and solar cells applications.

Bibliography

[J. M. Doyle et all] J. M. Doyle, B. Friedrich, J. Kim, and D. Patterson. Buffer-gas loading of atoms and molecules into a magnetic trap. Phys. Rev. A, 52:R2515, 1995. 5

[M. D. Di Rosa et all] M. D. Di Rosa. Laser-cooling molecules. Eur. Phys. J. D 31, 395 (2004).

[H. J. Metcalf et all] Laser Cooling and Trapping. Springer, Berlin 4

[Ahtee et al. 2009] Ahtee V., Merimaa M., & Nyholm K. 2009, OptL, **34**, 2619 20

[Amyay et al. 2011] Amyay, B., Fayt, A., & Herman, M. 2011, JChPh, **135**, 234305 27, 32

[Andersen et al. 1964] Andersen, H.C., Oppenheim, I., Shuler, K.E., & Weiss, G.H., 1964, JMP, **5**, 522 29

[Arteaga et al. 2007] Arteaga, S.W., Bejger, C.M., Gerecke, J.L., et al. 2007, JMoSp, **243**, 253 21

[Babay et al. 1998] Babay, A., Ibrahimi, M., Lemaire, V., et al. 1998, JQSRT, **59**, 195 21

[Ball & De Lucia 1998] Ball, C.D., & De Lucia, F.C. 1998, PhRvL, **81**, 305 22

[Bond et al. 2008] Bond, K.S., Collett, N.D., Fuller, E.P., et al. 2008, ApPhB, **90**, 255 21, 26

[Bouanich et al. 1991] Bouanich, J.P., Boulet, C., Blanquet, G., Walrand, J., & Lambot, D. 1991, JQSRT, **46**, 317 21

[Bovino et al. 2011] Bovino, S., Zhang, P., Kharchenko, V., & Dalgarno, A. 2011, JChPh, **135**, 024304 72

[Bradford et al. 2003] Bradford, C.M., T. Nikola, Stacey, A.D., et al. J. 2003, ApJ, **586**, 891 22

[Bulleid et al. 2013] Bulleid, N.E., Skoff, S.M., Hendricks, R.J., et al. 2013, PCCP, **15**, 12299 4, 22, 71

[Burgdorf et al. 2006] Burgdorf, M., Orton, G., van Cleve, J., Meadows, & V., Houck, J. 2006, Icar, **184**, 634 21

[Carr et al. 2009] Carr, L.D., DeMille, D., Krems, R.V., & Ye, J. 2009, NJPh, **11**, 055049 22, 71

[Carr et al. 2009] Carr, L.D., DeMille, D., Krems, R.V., & Ye, J. 2009, NJPh, **11**, 055049 1, 4

[Conrath et al. 1989] Conrath, B., Flasar, F.M., & Hanel, R., et al. 1989, Sci, **246**, 1454 2, 21

[Didriche et al. 2012] Didriche, K., Földes, T., Lauzin, C., et al. 2012, MolPh, **110**, 2781 20

[Edwards et al. 2005] Edwards, C.S., Barwood, G.P., Margolis, H.S., Gill, P., & Rowley, W.R.C. 2005, JMoSp, **234**, 143 20

[Hardwick et al. 2006] Hardwick, J.L., Martin, Z.T., Schoene, E.A., Tyng, V., & Wolf, E.N. 2006, JMoSp, **239**, 208 20

[Hitran] Harvard-Smithsonian Center for Astrophysics (CFA), Cambridge, MA & Zuev Insitute of Atmosperic Optics (IAO), Tomsk, RU: Hitran on the Web Information System 28

[Heijmen et al. 1999] Heijmen, T.G.A., Moszynski, R., Wormer, P.E.S., et al. 1999, JChPh, **111**, 2519 21

[Herman et al. 2007] Herman, M. 2007, MolPh, **105**, 2217 20

[Herman et al. 2003] Herman, M., Campargue, A., El Idrissi, M.I., Vander & Auwera, J. 2003, JChPh, Ref. Data **32**, 921 20

[Hutzler et al. 2012] Hutzler, N.R., Lu, H.-I., & Doyle, J.M. 2012, ChR, **112**, 4803 32

[Lellouch et al. 2009] Lellouch, E., Sicardy, B., de Bergh, et al. 2009, A&A, **495**, L17 72

[Lu et al. 2008] Lu, M. J., Hardman, K.S., Weinstein J.D., & Zygelman B. 2008, PhRvA, **77**, 060701(R) 33

[Lu & Weinstein 2009] Lu, M.-J., & Weinstein, J.D. 2009, NJPh, **11**, 055015 31

[Maddaloni book] Maddaloni, P., Bellini, M., & De Natale, P. 2013, Laser-based Measurements for Time and Frequency Domain Applications. A Handbook., (London:CRC Press, Taylor&Francis Group) 28, 32

[Maxwell 2005] Maxwell, S.E., Brahms, N., & deCarvalho, R., et al. 2005, PhRvL, **95**, 173201 2, 4, 35

[Mengel et al. 2000] Mengel, M., & De Lucia, F.C. 2000, ApJ, **543**, 271 22

[Messer & De Lucia 1984] Messer, J.K., & De Lucia, F.C. 1984, PhRvL, **53**, 2555 22

[Nan & Houston 1992] Nan, G., & Houston, P.L. 1992, JChPh, **97**, 7865 72

[Noll et al. 1986] Noll, K.S., Knacke, R.F., Tokunaga, A.T., et al. 1986, Icar, **65**, 257 2, 21

[Oancea et al. 2012] Oancea, A., Grasset, O., Le Menn, E., et al. 2012, Icar, **221**, 900 72

[Onstott et al. 2006] Onstott, T.C., McGown, D., Kessler, J., et al. 2006, AsBio, **6**, 377 72

[Oremland & Voytek 2008] Oremland, R.S., & Voytek, M.A. 2008, AsBio, **8**, 45 21

[Podolske & Loewenstein 1984] Podolske, J.R., & Loewenstein, M. 1984, JMoSp, **107**, 241 21

[Rinsland et al. 1987] Rinsland, C.P., Zander, R., Farmer, C.B., Norton, R.H., & Russell, J.M. 1987, JGR, **92**, 11951 20

[Rothman et al. 1998] Rothman, L.S., Rinsland, C.P., Goldman, A., et al. 1998, JQSRT, **60**, 665 27

[Ryu et al. 2008] Ryu, H.Y., Lee, S.H., Lee, W.K., Moon, H.S., & Suh, H.S. 2008, OExpr, **16**, 2867 20

[Sanna] Sanna, G., & Tomassetti, G. 2005, Introduction to Molecular Beam Gas Dynamics, (London:Imperial College Press) 28

[Santamaria et al. 2014] Santamaria, L., Di Sarno, V., Ricciardi, I., et al. 2014, JMoSp, **300**, 116

[Skoff et al. 2011] Skoff, S.M., Hendricks, R.J., Sinclair, C.D.J., et al. 2011, PhRvA, **83**, 023418 31, 33

[Stuhl et al. 2014] Stuhl, B.K., Hummon, M.T., & Ye, J. 2014, ARPC, **65**, 501

[Sushkov & Budker 2008] Sushkov, O., & Budker, D. 2008, PhRvA, **77**, 042707 33

[Thibault 2005] Thibault, F. 2005, JMoSp, **234**, 286 21

[Thibault et al. 2007] Thibault, F., Cappelletti, D., Pirani, F., Blanquet, G., & Bartolomei, M. 2007, EPJD, **44**, 337 20

[Thorpe et al. 2009] Thorpe, M.J., Adler, F., Cossel, K.C., de Miranda, M.H.G., & Ye, J. 2009, CPL, **468**, 1 20

[Valipour & Zimmermann 2001] Valipour, H., & Zimmermann, D. 2001, JChPh, **114**, 3535 21

[Varanasi 1992] Varanasi, P. 1992, JQSRT, **47**, 263 21

[Varanasi et al. 1983] Varanasi, P., Giver, L.P., & Valero, F.P.J. 1983, JQSRT, **30**, 497 2, 21

[Ziurys et al. 1994] Ziurys, L.M. , Apponi, A.J., Hollis, J.M., & Snyder, L.E. 1994, ApJ, **436**, L181 72

[Borner 2004] orner. Lect. Notes Phys. **648:21** 55

[Buchler 2007] Büchler and A. Micheli and P. Zoller. Nature Physics **3:726** 70

[Bagdonaite 2013] J. Bagdonaite and P. Jansen and C. Henkel and H.L. Bethlem and K.M. Menten and W. Ubachs. Scienc **82:055401** 56

[Bakalov 2010] D. Bakalov and V. Korobov and S. Schiller. Phys. Rev. A **82:055401** 56

[Barry 2012] F. Barry and E.S. Shuman and E.B. Norrgard and D. DeMille. Phys. Rev. Lett.**108:103002**

[Bethlem 2009] L. Bethlem and M. Kajita and B. Sartakov and G. Meijer and W. **163:55** 69

[Bethlem 2009] L. Bethlem and W. Ubachs. Faraday Discussions **142:25** 69

[Calmet 2002] X. Calmet and H. Fritzsch. Eur. Phys. **24:639** 58

[Carr et all.,2009] L.D. Carr and D. DeMille and R.V. Krems and J. Ye. New Journal of Physics **11:055049**

[Chiba 2011] T. Chiba Progress of Theoretical Physics**126:993** 56

[Chin 2009] C. Chin and V.V. Flambaum and M.G. Kozlov.New Journal of Physics**11:055048** 54

[Constantin 1999] F. Constantin and R.J. Butcher and P.E. Durand and A. Amy Klein and Ch. Chardonnet.Phys. Rev. A**60:R753** 50

[Calmet 2002] Cronin NaturePhys 2013 D. Cronin and W.F. Holmgren. Nature Physics **9:137**

[Darquie 2010] B. Darquie and C. Stoeffler and A. Shelkovnikov and C. Daussy and A. Amy-Klein and Ch. Chardonnet and S. Zrig and L. Guy and J. Crassous and P. Soulard and P. Asselin and T.R. Huet and P. Schwerdtfeger and R. Bast and T. Saue. Chirality **22:870** 69

[Dirac 1937] M. Dirac. Nature**139:323** 53

[Fritzsch 2004] H. Fritzsch. Lect. Notes Phys. **648:107** 68

[Heiner 2006] E. Heiner and H.L. Bethlem and G. Meijer. Physical Chemistry Chemical Physics **8:2666**

[Hummon 2013] T. Hummon and M. Yeo and B.K. Stuhl and A.L. Collopy and Y. Xia and J. Ye. Phys. Rev. Lett. **110:143001** 4

[Hutzler 2012] R. Hutzler and Hsin-I Lu and J.M. Doyle. Chemical Reviews **112:4803** xiii, 4, 43, 51, 60

[Ivanchik 2003] A. Ivanchik and P. Petitjean and E. Rodriguez and D. Varshalovich. Astrophysics and Space Science **283:583** 54

[Karshenboim 2002] G. Karshenboim. In "Time and Matter. Proceedings of the International Colloquium on the Science of Time" **26** 54

[Karshenboim 2004] G. Karshenboim56
. Lect. Notes Phys. **648:1**

[Kiefer 2004] C. Kiefer. Lect. Notes Phys. **648:115** 53, 68

[Kuma 2009] S. Kuma and T. Momose. New Journal of Physics **11:055023** 59

[Lea 2007] N. Lea .Rep. Prog. Phys. **70:1473** 55, 57

[Lev 2008] L. Lev and A. Vukics and E.R. Hudson and B.C. Sawyer and P. Domokos and H. Ritsch and J. Ye. Phys. Rev. A**77:023402**

[Lorini 2008] L. Lorini and N. Ashby and A. Brusch and S. Diddams and R. Drullinger and E. Eason and T. Fortier and P. Hastings and T. Heavner and D. Hume and W. Itano and S. Jefferts and N. Newbury and T. Parker and T. Rosenband and J. Stalnaker and W. Swann and D. Wineland and J. Bergquist. Eur. Phys. J. Special Topics **163:19** 57

[Marciano 2004] J. Marciano. ect. Notes Phys. **6483:97** 53

[Maxwell 2005] E. Maxwell and N. Brahms and R. deCarvalho and D.R. Glenn and J.S. Helton and S.V. Nguyen and D. Patterson and J. Petricka and D. DeMille and J.M. Doyle. Phys. Rev. Lett. **95:173201** 2, 4, 35

[Vandemeerakker 2008] T. van de Meerakker and H.L. Bethlem and G. Meijer. Nature Physics **4:595** 2

[Vandemeerakker 2012] T. van de Meerakker and H.L. Bethlem and N. Vanhaecke and G. Meijer. Chemical Reviews **112:4828** 62

[Micheli 2006] A. Micheli and G.K. Brennen and Zoller P.. Nature Physics **2:341** 70

[Mohr 2012] J. Mohr and B.N. Taylor and D.B. Newell55
Rev. Mod. Phys.**84:1527**

[Molaro 2010] P. Molaro. Highlights of Astronomy **15:326** 56

[Orzel 2012] C. Orzel. Phys. Scr. **86:068101** 52

[Osterwalder 2010] A. Osterwalder and S.A. Meek and G. Hammer and H. Haak and G. Meijer. Phys. Rev. A **81:051401(R)**

[Pizzocaro 2012] M. Pizzocaro and G. Costanzo and A. Godone and F. Levi and A. Mura and M. Zoppi and D. Calonico. IEEE Trans Ultrason Ferroelectr Freq Control.**59:426** 67

[Ramsey 1950] F. Ramsey. Phys. Rev. **78:695**

[Shelkovnikov 2008] A. Shelkovnikov and R.J. Butcher and C. Chardonnet and A. Amy-Klein.Phys. Rev. Lett.**100:150801** 4, 56, 67

[Stuhl 2012] K. Stuhl and M.T. Hummon and M. Yeo and G. Quemener and J. Bohn, and J. Ye. Nature **492:396**

[Tokunaga 2011] K. Tokunaga and W. Skomorowski and P.S. Zuchowski and R. Moszynski and J.M. Hutson and E.A. Hinds and M.R. Tarbutt. Eur. Phys. J. D **65:141**

[Uzan 2003] P. Uzan.Rev. Mod. Phys.**75:403** 53

[Zeppenfeld 2012] M. Zeppenfeld and U. Englert and R. Ockner and A. Prehn and M. Mielenz and C. Sommer and L.D. van Buuren and M. Motsch and G. Rempe. Nature **491:570**

[Calmet 2002] Calmet 2002 X. Calmet and H. Fritzsch. Eur. Phys. J. C
24:639

[Ahtee et al. 2009] Ahtee V., Merimaa M., & Nyholm K. 2009, OptL, **34**, 2619 20

[Amyay et al. 2011] Amyay, B., Fayt, A., & Herman, M. 2011, JChPh, **135**, 234305 27, 32

[Andersen et al. 1964] Andersen, H.C., Oppenheim, I., Shuler, K.E., & Weiss, G.H., 1964, JMP, **5**, 522 29

[Arteaga et al. 2007] Arteaga, S.W., Bejger, C.M., Gerecke, J.L., et al. 2007, JMoSp, **243**, 253 21

[Babay et al. 1998] Babay, A., Ibrahimi, M., Lemaire, V., et al. 1998, JQSRT, **59**, 195 21

[Ball & De Lucia 1998] Ball, C.D., & De Lucia, F.C. 1998, PhRvL, **81**, 305 22

[Bond et al. 2008] Bond, K.S., Collett, N.D., Fuller, E.P., et al. 2008, ApPhB, **90**, 255 21, 26

[Bouanich et al. 1991] Bouanich, J.P., Boulet, C., Blanquet, G., Walrand, J., & Lambot, D. 1991, JQSRT, **46**, 317 21

[Bovino et al. 2011] Bovino, S., Zhang, P., Kharchenko, V., & Dalgarno, A. 2011, JChPh, **135**, 024304 72

[Bulleid et al. 2013] Bulleid, N.E., Skoff, S.M., Hendricks, R.J., et al. 2013, PCCP, **15**, 12299 4, 22, 71

[Burgdorf et al. 2006] Burgdorf, M., Orton, G., van Cleve, J., Meadows, & V., Houck, J. 2006, Icar, **184**, 634 21

[Conrath et al. 1989] Conrath, B., Flasar, F.M., & Hanel, R., et al. 1989, Sci, **246**, 1454 2, 21

[Didriche et al. 2012] Didriche, K., Földes, T., Lauzin, C., et al. 2012, MolPh, **110**, 2781 20

[Edwards et al. 2005] Edwards, C.S., Barwood, G.P., Margolis, H.S., Gill, P., & Rowley, W.R.C. 2005, JMoSp, **234**, 143 20

[Hardwick et al. 2006] Hardwick, J.L., Martin, Z.T., Schoene, E.A., Tyng, V., & Wolf, E.N. 2006, JMoSp, **239**, 208 20

[Hitran] Harvard-Smithsonian Center for Astrophysics (CFA), Cambridge, MA & Zuev Insitute of Atmosperic Optics (IAO), Tomsk, RU: Hitran on the Web Information System 28

[Heijmen et al. 1999] Heijmen, T.G.A., Moszynski, R., Wormer, P.E.S., et al. 1999, JChPh, **111**, 2519 21

[Herman et al. 2007] Herman, M. 2007, MolPh, **105**, 2217 20

[Herman et al. 2003] Herman, M., Campargue, A., El Idrissi, M.I., Vander & Auwera, J. 2003, JChPh, Ref. Data **32**, 921 20

[Lellouch et al. 2009] Lellouch, E., Sicardy, B., de Bergh, et al. 2009, A&A, **495**, L17 72

[Lu et al. 2008] Lu, M. J., Hardman, K.S., Weinstein J.D., & Zygelman B. 2008, PhRvA, **77**, 060701(R) 33

[Lu & Weinstein 2009] Lu, M.-J., & Weinstein, J.D., Cold TiO($X^3\Delta$)-He collisions 2009, NJPh, **11**, 055015 31

[Maxwell et al. 2005] Maxwell, S.E., Brahms, N., & deCarvalho, R., et al. 2005, PhRvL, **95**, 173201 22, 71

[Mengel et al. 2000] Mengel, M., & De Lucia, F.C. 2000, ApJ, **543**, 271 22

[Messer & De Lucia 1984] Messer, J.K., & De Lucia, F.C. 1984, PhRvL, **53**, 2555 22

[Nan & Houston 1992] Nan, G., & Houston, P.L. 1992, JChPh, **97**, 7865 72

[Noll et al. 1986] Noll, K.S., Knacke, R.F., Tokunaga, A.T., et al. 1986, Icar, **65**, 257 2, 21

[Oancea et al. 2012] Oancea, A., Grasset, O., Le Menn, E., et al. 2012, Icar, **221**, 900 72

[Onstott et al. 2006] Onstott, T.C., McGown, D., Kessler, J., et al. 2006, AsBio, **6**, 377 72

[Oremland & Voytek 2008] Oremland, R.S., & Voytek, M.A. 2008, AsBio, **8**, 45 21

[Podolske & Loewenstein 1984] Podolske, J.R., & Loewenstein, M. 1984, JMoSp, **107**, 241 21

[Rinsland et al. 1987] Rinsland, C.P., Zander, R., Farmer, C.B., Norton, R.H., & Russell, J.M. 1987, JGR, **92**, 11951 20

[Rothman et al. 1998] Rothman, L.S., Rinsland, C.P., Goldman, A., et al. 1998, JQSRT, **60**, 665 27

[Ryu et al. 2008] Ryu, H.Y., Lee, S.H., Lee, W.K., Moon, H.S., & Suh, H.S. 2008, OExpr, **16**, 2867 20

[Sanna] Sanna, G., & Tomassetti, G. 2005, Introduction to Molecular Beam Gas Dynamics, (London:Imperial College Press) 28

[Santamaria et al. 2014] Santamaria, L., Di Sarno, V., Ricciardi, I., et al. 2014, JMoSp, **300**, 116

[Skoff et al. 2011] Skoff, S.M., Hendricks, R.J., Sinclair, C.D.J., et al. 2011, PhRvA, **83**, 023418 31, 33

[Stuhl et al. 2014] Stuhl, B.K., Hummon, M.T., & Ye, J. 2014, ARPC, **65**, 501

[Sushkov & Budker 2008] Sushkov, O., & Budker, D. 2008, PhRvA, **77**, 042707 33

[Thibault 2005] Thibault, F. 2005, JMoSp, **234**, 286 21

[Thibault et al. 2007] Thibault, F., Cappelletti, D., Pirani, F., Blanquet, G., & Bartolomei, M. 2007, EPJD, **44**, 337 20

[Thorpe et al. 2009] Thorpe, M.J., Adler, F., Cossel, K.C., de Miranda, M.H.G., & Ye, J. 2009, CPL, **468**, 1 20

[Valipour & Zimmermann 2001] Valipour, H., & Zimmermann, D. 2001, JChPh, **114**, 3535 21

[Varanasi 1992] Varanasi, P. 1992, JQSRT, **47**, 263 21

[Varanasi et al. 1983] Varanasi, P., Giver, L.P., & Valero, F.P.J. 1983, JQSRT, **30**, 497 2, 21

[Ziurys et al. 1994] Ziurys, L.M. , Apponi, A.J., Hollis, J.M., & Snyder, L.E. 1994, ApJ, **436**, L181 72

[de Angelis 1995] de Angelis M., Gagliardi G., Gianfrani L. and G.M. Tino 1995, PRL, **76**, 2840

[Hilborn 1996] Hilborn, R.C., Yuca C.L., L.E. 1996, PRL, **76**, 2844

[Berden 1998] Berden G., Enlgen R.,P.C.M. Christianen, J.C. Maan and G. Meijer 1998, PRA, **58**, 3114

[Sikivie 2014] Sikivie 2014 , PRL, **113**, 201301

[Hutzler et al. 2012] Hutzler, N.R., Lu, H.-I., & Doyle, J.M. 2012, ChR, **112**, 4803 32

[de Carvalho 1999] de Carvalho, R., Doyle J.M., Friedrich B., Guillet T., Kim J., Patterson D., Weinstein J.D. 1999, EUR. Phys J. D **7**, 289

[OKeefe et al. 1988] A. OKeefe and D.A.G. Deacon Cavity ring-down optical spectrometer for absorption measurements using pulsed laser sources Rev. Sci. Instrum. 59, 2544 (1988) 36

[Romanini et al. 1997] D. Romanini, A.A. Kachanov, N. Sadeghi and F. Stoeckel CW cavity ring down spectroscopy Chem. Phys. Lett. 264, 316 (1997) 36

[Mazurenka et al. 2005] M. Mazurenka, A.J. Orr-Ewing, R. Peverall and G.A.D. Ritchie Cavity ring-down and cavity enhanced spectroscopy using diode lasers Annu. Rep. Prog. Chem., Sect. C 101, 100-142 (2005) 36

[Lehmann et al. 1996] K.K. Lehmann and D. Romanini The superposition principle and cavity ring-down spectroscopy J. Chem. Phys. 105, 15 (1996) 36

[Scoles 1988] G. Scoles, D. Bassi, U. Buck, and D. C. Laine, eds., Atomic and Molecular Beam Methods, vol. 1 (Oxford University Press, 1988). 3

[Scoles 1992] G. Scoles, D. C. Laine, and U. Valbusa, eds., Atomic and Molecular Beam Methods, vol. 2 (Oxford University Press, 1992). 3

[Demtroder 2008] Demtröder, Laser Spectroscopy, vol. 2: Experimental techniques (Springer, 2008), 4th ed.

[Patterson 2007] D. Patterson and S. M. Doyle, The Journal of Chemical Physics **126**, 154307 (2007). 4

[Sommer 2009] C. Sommer, L. D. van Buuren, M. Motsch, S. Pohle, J. Bayerl, P. W. H. Pinkse, and G. Rempe, Faraday Discussions **142**, 203 (2009). 4

[Bethlem 1999] H. L. Bethlem, G. Berden, and G. Meijer, Physical Review Letters **83**, 1558 (1999). 4

[vandeMeerakker 2008] S. Y. T. van de Meerakker, H. L. Bethlem, and G. Meijer, Nature Physics **4**, 595 (2008). 4

[vandeMeerakker 2012] S. Y. T. van de Meerakker, H. L. Bethlem, N. Vanhaecke, and G. Meijer, Chemical Reviews **112**, 4828 (2012). 4

[Zeppenfeld 2012] M. Zeppenfeld, B. G. U. Englert, R. Glöckner, A. Prehn, M. Mielenz, C. Sommer, L. D. van Buuren, M. Motsch, and G. Rempe, Nature **491**, 570 (2012). 4

[Prehn 2016] A. Prehn, M. Ibrügger, R. Glöckner, G. Rempe, and M. Zeppenfeld, Physical Review Letters **116**, 063005 (2016). 4

[Shuman 2010] E. S. Shuman, J. F. Barry, and D. DeMille, Nature **467**, 820 (2010). 4

[Isaev 2016] T. A. Isaev and R. Berger, Physical Review Letters **116**, 063006 (2016). 4

[Hummon 2013] M. T. Hummon, M. Yeo, B. K. Stuhl, A. L. Collopy, Y. Xia, and J. Ye, Physical Review Letters **110**, 143001 (2013). 4

[Norrgard 2016] E. B. Norrgard, D. J. McCarron, M. H. Steinecker, M. R. Tarbutt, and D. DeMille, Physical Review Letters **116**, 063004 (2016). 4

[Maddaloni book] P. Maddaloni, M. Bellini, and P. De Natale, Laser-based measurements for time and frequency applications. A handbook (Taylor and Francis Group, 2013). 4, 39

[Hudson 2011] J. J. Hudson, D. M. Kara, I. J. Smallman, B. E. Sauer, M. R. Tarbutt, and H. E. A., Nature **473**, 493 (2011). 4

[Baron 2013] J. Baron, W. C. Campbell, D. DeMille, J. M. Doyle, G. Gabrielse, Y. V. Gurevich, P. W. Hess, N. R. Hutzler, E. Kirilov, I. Kozyryev, et al., Science **343**, 269 (2013). 4

[Shelkovnikov 2008] A. Shelkovnikov, R. J. Butcher, C. Chardonnet, and A. Amy-Klein, Physical Review Letters **100**, 150801 (2008). 4, 56, 67

[Ubachs 2016] W. Ubachs, J. Bagdonaite, E. J. Salumbides, M. T. Murphy, and L. Kaper, arXiv:1511.04476 (2016). 4

[Tokunaga 2013] S. K. Tokunaga, C. Stoeffler, F. Auguste, A. Shelkovnikov, C. Daussy, A. Amy-Klein, C. Chardonnet, and B. Darquié, Molecular Physics **111**, 2363 (2013). 4

[Stoll 2008] M. Stoll, J. M. Bakker, T. C. Steimle, G. Meijer, and A. Peters, Physical Review A **78**, 032707 (2008). 35

[Yeo 2015] M. Yeo, M. T. Hummon, A. L. Collopy, B. Yan, B. Hemmerling, E. Chae, J. M. Doyle, and J. Ye, Physical Review Letters **114**, 223003 (2015). 35

[Barry 2011] J. F. Barry, E. S. Shuman, and D. DeMille, Physical Chemistry Chemical Physics **13**, 18936 (2011). 35

[Patterson 2009] D. Patterson, J. Rasmussen, and J. M. Doyle, New Journal of Physics **11**, 055018 (2009). 35

[Santamaria 2015] L. Santamaria, V. Di Sarno, I. Ricciardi, M. De Rosa, S. Mosca, G. Santambrogio, P. Maddaloni, and P. De Natale, The Astrophysical Journal **801**, 50 (2015). 42, 49

[Santamaria 2014] L. Santamaria, V. Di Sarno, I. Ricciardi, S. Mosca, M. De Rosa, G. Santambrogio, P. Maddaloni, and P. De Natale, Journal of Molecular Spectroscopy **300**, 116 (2015). 43

[Romanini] D. Romanini, I. Ventrillard, G. Méjean, and E. Kerstel, Cavity-Enhanced Spectroscopy and Sensing (Springer-Verlag Berlin Heidelberg, 2014), vol. 179 of Springer Series in Optical Sciences, chap. Introduction to Cavity Enhanced Absorption Spectroscopy. 45

[Maddaloni 2010] P. Maddaloni, P. Malara, E. De Tommasi, M. De Rosa, I. Ricciardi, G. Gagliardi, F. Tamassia, G. Di Lonardo, and P. De Natale, The Journal of Chemical Physics **133**, 154317 (2010). 46

[Berden 2000] G. Berden, R. Peeters, and G. Meijer, International Reviews in Physical Chemistry **19**, 565 (2000). 46

[Ramsey 1950] N. F. Ramsey, Physical Review **78**, 695 (1950). 58

[Constantin 1999] L. F. Constantin, R. J. Butcher, P. E. Durand, A. Amy-Klein, and C. Chardonnet, Physical Review A **60**, R753 (1999). 50

[Amy-Klein 1999] A. Amy-Klein, L. F. Constantin, R. J. Butcher, C. Daussy, P. E. Durand, G. Nogues, and C. Chardonnet, Optics Express **4**, 67 (1999).

[Calonico 2014] D. Calonico, E. K. Bertacco, C. E. Calosso, C. Clivati, G. A. Costanzo, M. Frittelli, A. Godone, A. Mura, N. Poli, D. V. Sutyrin, et al., Applied Physics B: Lasers and Optics **117**, 979 (2014). 50

[Adler 2010] F. Adler, M. J. Thorpe, K. C. Cossel, and J. Ye, Annual Review of Analytical Chemistry **3**, 175 (2010). 73

[Maddaloni 2013] P. Maddaloni, M. Bellini, and P. De Natale, Laser-based measurements for time and frequency applications. A handbook (Taylor and Francis Group, 2013). 18, 69

[Maddaloni 2009] P. Maddaloni, P. Cancio, and P. De Natale, Measurement Science and Technology **20**, 052001 (2009). 44

[Morse 1996] Morse, M. D. In Atomic, Molecular, and Optical Physics: Atoms and Molecules; Dunning, F. B., Hulet, R. G., Eds.; Experimental Methods in the Physical Sciences; Academic Press: San Diego, CA, 1996; Vol. 29, Part B. p 21. 4

[Sebastiaan 2008] Sebastiaan Y. T. van de Meerakker1, Hendrick L. Bethlem1,2 Gerard Meijer, Taming molecular beams, Nature Physics 4, 595 - 602 (2008)

[Christen 2010] Wolfgang Christen, Klaus Rademann, Uzi Even, Supersonic Beams at High Particle Densities: Model Description beyond the Ideal Gas Approximation, J. Phys. Chem. A 2010, 114, 1118911201 12

[Bart Wit] Bart Wit, Defects in Pentacene Thin Films Grown by Supersonic Molecular Beam Deposition 13

[Kallmann 1921] H. Kallmann and F. Reiche Zeitschrift fr Physik A Hadrons and Nuclei, 1921, Volume 6, Number 1, pp. 352375 3

[Zeitschrift 1927] Zeitschrift fr Physik A Hadrons and Nuclei Volume 44, Numbers 45 (1927), 261268 3

[Rabi et all 1939] I. I. Rabi, S. Millman, and P. Kusch J. R. Zacharias, The Molecular Beam Resonance Method for Measuring Nuclear Magnetic Moments. The Magnetic Moments of 3Li6, 3Li7 and 9F19" Phys. Rev. 55, 526535 (1939) 3

[Herschbach 1976] D. R. Herschbach, Molecular Dynamics Of Chemical Reactions , Pure AppL Chem., Vol. 47, pp. 6173. Pergamon Press, 1976 3

[Gordon et all 1954] J. P. Gordon, H. J. Zeiger, and C. H. Townes, Molecular Microwave Oscillator and New Hyperfine Structure in the Microwave Spectrum of NH3" , Phys. Rev. 95, 282284 (1954) doi:10.1103/PhysRev.95.282 3

[Tatti et all 2015] Tatti, Aversa, Verucchi, Cavaliere, Garberoglio, M. Pugno, Speranza, Taioli, Towards room-temperature single-layer graphene synthesis by C60 Supersonic Molecular Beam Epitaxy 15

[Wessel and Lew 1953] Gnter Wessel and Hin Lew Phys. Hyperfine Structures of Silver and Gold by the Atomic Beam Magnetic Resonance Method, Rev. 92, 641. 1953 17

[Pauly 2000] Hans Pauly, Springer Science Business Media, 05 giu 2000 Atom, Molecule, and Cluster Beams I 17

[Danman et all 2005] M. F. Danman, L. Casalis, and G. Scoles, Supersonic molecular beam deposition of pentacene thin films on two Ag(111) surfaces with different step densities, Phys. Rev. B 72, 085404 2005 16

[Xia et all 1995] , Jones, Maity and Engstrom, Supersonic molecular beam scattering as a probe of thin film deposition processes, J, Vac. Sci. Technol. A 13, 2651 (1995) 16

[Podest et all 2000] , A. Podest, T. Toccoli, P. Milani, A. Boschetti, S. Innotta, Highly ordered growth of -quaterthiophene films by seeded supersonic molecular beam deposition: a morphological study, Surface Science, Vol 464, Issue 1, 20 September 2000, Pages L673L680 17

[Hutzler et all 2012] Nicholas R. Hutzler, Hsin-I Lu, and John M. Doyle, The Buffer Gas Beam: An Intense, Cold, and Slow Source for Atoms and Molecules, Chem. Rev. 2012, 112, 48034827 12

[Maddaloni 2009] P Maddaloni, P Cancio and P De Natale, Optical comb generators for laser frequency measurement, Meas. Sci. Technol. 20 (2009) 052001 (19pp) 41

Publications

Assessing the time constancy of the proton-to-electron mass ratio by precision ro-vibrational spectroscopy of a cold molecular beam. *L. Santamaria, V. Di Sarno, I. Ricciardi, S. Mosca, M. De Rosa, P. Maddaloni, P. De Natale.* Journal of Molecular Spectroscopy 300, 116 (2014).

Low-temperature spectroscopy of the $C_2H_2(v_1 + v_3)$ band in a helium buffer gas. *L. Santamaria, V. Di Sarno, I. Ricciardi, M. de Rosa , S. Mosca, G. Santambrogio, P. De Natale.* The Astrophysical Journal, 801, 50 (2015).

Axion dark matter detection by laser spectroscopy of ultracold molecular oxygen: a proposal. *l. Santamaria ; C. Braggio ; G. Carugno ; V. Di Sarno; P. Maddaloni; G. Ruoso.* New Journal of Physics, Volume 17 (2015).

Frequency-comb-assisted precision laser spectroscopy of CHF_3 around 8.6 μ m. *Alessio Gambetta, Nicola Coluccelli, Marco Cassinerio, Toney Teddy Fernandez, Davide Gatti, Antonio Castrillo, Adina Ceausu-Velcescu, Eugenio Fasci, Livio Gianfrani, Luigi Santamaria, Valentina Di Sarno, Pasquale Maddaloni, Paolo De Natale, Paolo Laporta and Gianluca Galzerano.* The Journal of Chemical Physics 143, 234202 (2015).

Comb-assisted cavity ring-down spectroscopy of a buffer-gas molecular beam. *L. Santamaria, V. Di Sarno, M. De Rosa, S. Mosca, I. Ricciardi, P. De Natale, D. Calonico, F. Levi, M. Inguscio, and P. Maddaloni.* Submitted to Physical Review Letters (2016).